Rochester Institute of Technology

RIT Digital Institutional Repository

Theses

5-1-2008

Nanomaterial synthesis and characterization for energy storage and conversion devices

Roberta A. DiLeo

Follow this and additional works at: https://repository.rit.edu/theses

Recommended Citation

DiLeo, Roberta A., "Nanomaterial synthesis and characterization for energy storage and conversion devices" (2008). Thesis. Rochester Institute of Technology. Accessed from

This Thesis is brought to you for free and open access by the RIT Libraries. For more information, please contact repository@rit.edu.

Nanomaterial Synthesis and Characterization for Energy Storage and Conversion Devices

By

Roberta A. DiLeo

We, the undersigned members of the Faculty of the Rochester Institute of Technology, certify that we have advised and/or supervised the candidate on the work described in this dissertation. We further certify that we have reviewed the dissertation manuscript and approve it in partial fulfillment of the requirements of the degree of Masters of Science in Materials Science & Engineering.

Approved by:

Dr. Ryne P. Raffaelle _____

Dr. John Andersen _____

Dr. Gerald Takacs _____

Materials Science & Engineering
Rochester Institute of Technology
May 2008

NANOMATERIAL SYNTHESIS AND CHARACTERIZATION FOR ENERGY STORAGE AND CONVERSION DEVICES

by

ROBERTA A. DILEO

A THESIS

Submitted in partial fulfillment of the requirements
for the degree of Masters of Science
in
Materials Science & Engineering
of the College of Science
at the
Rochester Institute of Technology

May 9, 2008

ABSTRACT

College of Science
Rochester Institute of Technology

Degree: Masters of Science Program: Materials Science & Engineering
Name of Candidate: Roberta A. DiLeo
Title: **Nanomaterial Synthesis and Characterization for Energy Storage and Conversion Devices**

Synthesis conditions and characterization techniques were investigated for a variety of nanomaterials that have potential for use in a plethora of energy storage and conversion devices, such as photovoltaics, thermionic emitters, lithium-ion batteries, and PEM fuel cells. A portion of this work focused on the development of a chemical vapor deposition synthesis technique for multi-walled carbon nanotubes (MWNTs) using an iron dimer in xylene as a liquid catalyst precursor. The optimization of synthesis conditions for this technique was subsequently followed by the development of a quantitative purity assessment method for MWNTs from Raman spectroscopy, which involves the ratios of peak heights in Raman spectra. Initial work in the development of this purity assessment method was extended to a second Raman excitation energy, and a universal equation of purity was developed for two excitation laser energies. The capability exists to develop free-standing electrode papers from these synthesized MWNTs for several of the aforementioned applications. A large portion of this work also focused on the characterization of materials commonly used in organic solar cells with the technique of cyclic voltammetry. Electrochemical measurements of semi-conducting CdSe quantum dots, fullerene derivatives, and polymers (MEH-PPV, P3HT, and MDMO-PPV) were completed to determine the band gap, ionization potential, and electron affinity of these materials in order to improve device fabrication by offering the capability of pre-selecting the materials incorporated in a given composite. This reduces time, energy, and expenses involved with fabrication, along with furthering the understanding of interactions between materials in a composite at the electronic level. This work has offered important contributions to the field of alternative energy by making strides in synthesizing, characterizing, and selecting appropriate materials for use in energy storage and conversion devices.

ACKNOWLEDGEMENTS

I wish to acknowledge the sponsored research programs in support of my research at the NanoPower Research Laboratories funded by BP solar, NASA, Air Force Research Laboratories, and the Department of Defense. I would also like to thank the R.I.T Honor's Program and the Barry M. Goldwater Scholarship and Excellence in Education Foundation for financial support during this degree.

I wish to thank the support of the professors who served on my committee:

Dr. John Andersen
Dr. Gerald Takacs

I would like to express my gratitude to the following individuals who I interacted with during my education as either colleagues or mentors:

Mr. William Van Derveer
Ms. Annick Anctil
Mr. Chris Schaureman
Mr. Corey Cress

I am especially thankful to Dr. Brian Landi who has been a wealth of knowledge, ideas, and advice as I have journeyed through this research and education venture. His counsel has been of utmost worth.

I would like to thank Dr. Ryne Raffaelle, whose zeal and determination "to enhance the performance of energy conversion and storage devices through the development of nanomaterials," made this work possible. I have benefited from a tremendous amount of opportunities with him as my advisor.

Finally, I wish to thank my family and friends for their love and support through this endeavor. I have been blessed with abilities and talents to accomplish this work and even more than that, wonderful, loving people to share my accomplishments with. To Sarah, my sister: your patience, love, and wisdom have been of tremendous value. To my parents, who have always loved and supported me, I thank you for the example you are to me and how you have motivated me to become who I can be.

TABLE OF CONTENTS

LIST OF FIGURES

CHAPTER 1 INTRODUCTION

A. Motivation

The field of nanotechnology is emerging as a driving force in research as technologies become smaller, faster, and more sustainable. This is particularly true in the development of materials for energy conversion and storage devices, such as organic photovoltaics, lithium-ion batteries, proton exchange membrane (PEM) fuel cells, and thermionic power devices (Figure 1) [1, 2]. With the current energy challenges technology is facing [3], an alternative to typical materials is being sought. One plausible solution is the use of nanomaterials. Nanomaterials are a broad class of materials ranging from organic carbon species to inorganic quantum dots, where the materials exhibit a large range of advantageous properties. Universally, nanomaterials are influenced by quantum confinement effects in some manner depending on their dimensions [4]. These unique properties that arise due to size

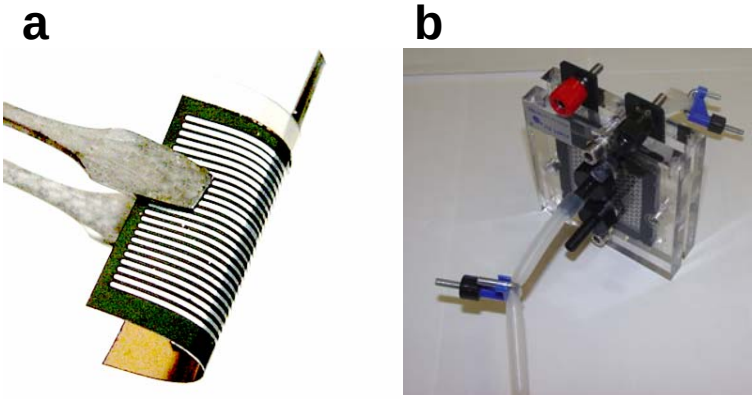

Figure 1. Energy conversion and storage devices employing nanomaterials: (a) flexible quantum dot-organic photovoltaic and (b) nanotube electrode PEM fuel cell set-up.

effects are emphasized in the utility of nanomaterials as opposed to the attributes of the bulk materials. The fundamental understanding of material characterization and how material electronic properties are affected by synthesis is vital to the successful implementation of these nanomaterials into current energy storage and conversion devices. A component of this work investigates the properties, as influenced by synthesis, of multi-walled carbon nanotubes which can be used in battery, PEM fuel cell membranes, and thermionic applications. Another element of this work focused on the characterization of semiconducting quantum dots and fullerene derivatives for use in organic photovoltaics. It is imperative for novel designs and materials to be implemented for continued progress in photovoltaic performance. An important aspect of photovoltaics is proper material selection since photovoltaic performance depends largely on maximizing photon absorption, exciton diffusion, exciton dissociation, and carrier transport, which are all influenced by individual material properties [5]. Similarly, the principles of band structure and energy level alignment are significant to the development of well performing devices as they promote efficient charge dissociation and charge transfer within the device. The enhancement of photon absorption in a device can be accomplished by selecting materials with appropriate band gaps to absorb the solar spectrum. Also of importance is the minimization of recombination sites within the bulk heterojunction. This can be done by avoiding materials which will cause traps due to unsuitable energy level alignment. Due to the tunability of quantum dot band gaps, they are useful candidates for incorporation in organic photovoltaics. This investigation of materials for organic photovoltaics was expanded to include the polymers which are typically used

in the solar cell composites. It was advantageous to thoroughly characterize the polymers as well as the materials that were to be blended into the composite to have a more complete understanding of material properties within a device.

B. Nanomaterials for Energy Storage and Conversion Devices

(i) Multi-walled Carbon Nanotubes

One nanomaterial that has been under extensive investigation since its discovery is the multi-walled carbon nanotube (MWNT) [6]. A single walled nanotube can be envisioned as a graphene sheet rolled into a seamless cylinder. A MWNT is a collection of concentric cylinders each with a slightly larger diameter and an interlayer spacing (Figure 2). Due to their unique mechanical, electrical, and chemical properties, MWNTs have been investigated to discover their utility in devices [1, 7-9]. Specifically, aligned arrays of MWNTs have been used in the fabrication of solar cells, lithium-ion batteries, sensors, and integrated circuits, among other devices [7-9]. As a result of the significant role MWNTs can play in device

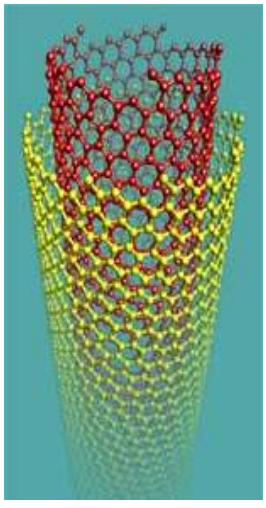

Figure 2. Multi-walled carbon nanotube.

composition, it is important to quantify the quality of material incorporated in a given device fabrication process. This will allow repeatable and reliable measurements concerning the effect MWNTs have on device performance. This quantification is also a necessary step because regardless of the synthesis technique (laser vaporization, arc discharge, or chemical vapor deposition), the resulting material is a mixture of both nanotubes and amorphous carbon species. For optimum device performance, high quality nanotubes are desired as opposed to amorphous carbon. Therefore a simple method to determine the quality of nanotubes in a sample, much like the method developed for single-wall carbon nanotubes, is advantageous [10]. While many techniques exist as possible characterization methods, including scanning electron microscopy (SEM), transmission electron microscopy (TEM), thermogravimetric analysis (TGA), and Raman spectroscopy, the proper combination of these techniques (or others) to produce a protocol for quantifying MWNT purity (defined as the mass fraction of nanotubes in a sample) has yet to be established [11-16]. Commonly used microscopy techniques can be quite useful at quantifying nanotube diameter or interlayer spacing. However, these methods provide a qualitative understanding of the MWNT purity as they are limited in their ability to determine other factors affecting purity (e.g. degree of carbonaceous coatings, encapsulated metal particles, etc.). While TGA can accurately quantify a sample's metal content, the decomposition curve cannot easily be deconvolved to provide carbonaceous MWNT purity. Attempts to use Raman spectroscopy for purity assessment have relied upon a ratio of the D-band peak (~1350 cm^{-1}) and the G-band

peak (~1580 cm^{-1}) to infer a purity level. However with no reference for comparison, ambiguity arises in the interpretation of data for these two peaks from the effects that carbon impurities have on the bands' intensities. Therefore, a ratio containing the G'-band peak (~2700 cm^{-1}) may represent a more accurate measurement of MWNT quality or purity, since the G' band resonant Raman intensity is dramatically enhanced in the case of carbon nanotubes[17]. In this work, a method of purity assessment using Raman spectroscopy, in conjunction with SEM, TEM, and TGA, for MWNTs is discussed. This work includes the purity assessment using two excitation lasers, 1.96 eV and 2.54 eV, and discusses the utility of using the $I_{G'}/I_D$ as a method of determining quantitative purity values for MWNTs. The purity assessment method also extends beyond bulk MWNT characterization to determining purity of MWNT aligned arrays.

(ii) Semiconducting Quantum Dots

The unique capability of quantum dots to be electronically tuned to a specific band gap is a potentially beneficial characteristic to employ in photovoltaics. Widely known are the bulk properties of certain materials that change when the given materials are constrained in size. For quantum dots, which are 3 dimensional wells and 0 dimensional conductors, quantum confinement effects influence the material's optoelectronic properties. In analogy to a particle in a box (Figure 3), the allowed energy levels within a quantum dot will change accordingly with its diameter. This allows for the ability to synthesize band-gap specific materials to absorb particular

wavelengths of the solar spectrum. In this work a series of colloidal cadmium selenide quantum dots ranging in size were synthesized.

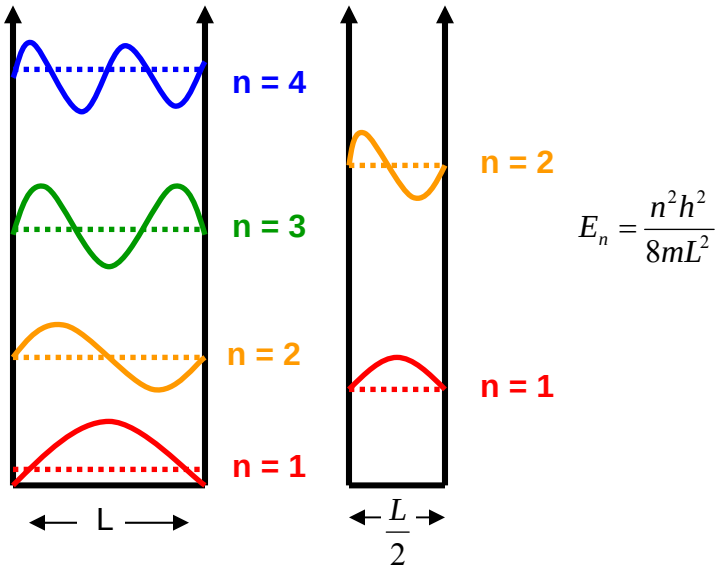

Figure 3. Diagram depicting the effects of quantum confinement. As a spatial dimension is changed, the energy levels of the material change accordingly. The equation for a particle in a box is shown, which is often used as a reference for energetic behavior in nanomaterials.

(iii) Fullerenes

Fullerene derivatives offer unique advantages to organic photovoltaics as well. Fullerenes are often incorporated to act as a charge dissociation site within the device because of their ability to attract and hold more than one extra electron within their structures. The cage of the fullerenes, as well as any substituent groups that are added to the cage, acts as charge dissociation centers. Figure 4 depicts some of the more commonly used fullerene derivatives in organic photovoltaics: [11]-phenyl C_{61} butyric acid methyl ester (PCBM C_{60}), [6,6]-phenyl C71 butyric acid methyl ester

(PCBM C_{70}), 1-3-methoxycarbonyl propyl-1-thienyl- 6,6 –methanofullerene (ThCBM C_{60}), and phenyl-C61-butyric acid (PCBA C_{60}).

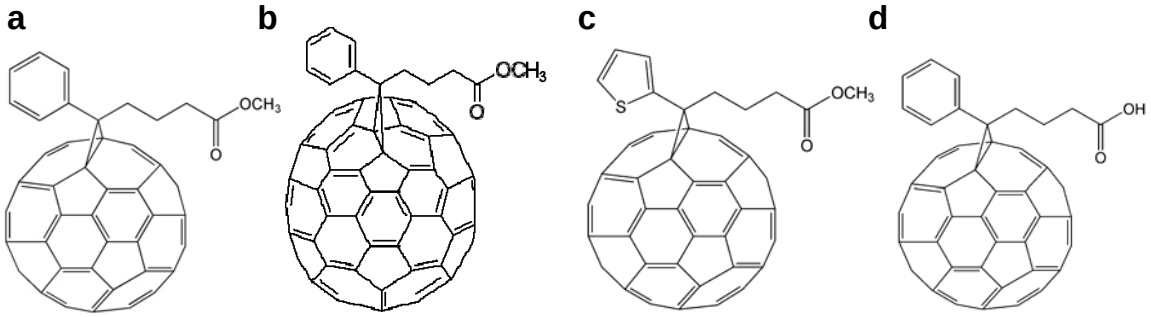

Figure 4. Molecular structure of (a) PCBM C_{60}, (b) PCBM C_{70}, (c) ThCBM C_{60}, and (d) PCBA C_{60}.

(iv) Polymer Composites

In organic photovoltaic research, there is a constant need to develop new materials, in particular polymers, which have optimal band gaps for absorption, dissociation, and collection of charges. The three commonly used polymers, which are sufficient for the current state-of-the-art organic devices, are MEH-PPV (Poly[2-methoxy-5-(2-ethylhexyloxy)-1,4-phenylenevinylene]), P3HT (Poly(3-hexylthiophene-2,5-diyl)) and MDMO-PPV (Poly[2-methoxy-5-(3′,7′-dimethyloctyloxy)-1,4-phenylenevinylene]) (Figure 5). Since the polymer is the base of any composite used for the active layer, it is essential to have an understanding of its energy levels. If material energy levels cannot be properly aligned to a given polymer, either a different polymer must be selected or a new set of nanomaterials must be used to incorporate into the polymer matrix. Several research papers have reported on the electrochemistry of nanomaterials and polymers commonly used in

organic photovoltaics[18-21]. In this work these three polymers are focused on, exhibiting favorable band gaps, and offering an array of structures to suit an assortment of nanomaterials in a matrix.

Examining the polymer composites using cyclic voltammetry extended this research and gave a more complete understanding of the interactions that occur within the composite. This work was consistent with other research investigating the properties of composites[22-24]. Another extension of this work also arose by investigating the composites both in the dark and under illumination which gave insight as to the behavior of the composite under a representative environment for a working device, an essential step in the investigation of energy band alignment. Also important is the investigation of composite properties using this technique to have a thorough understanding of the interactions that occur in devices and their impact on band structure.

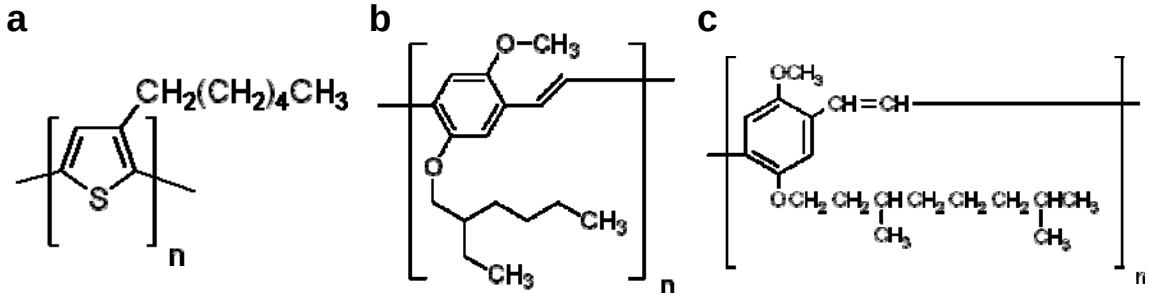

Figure 5. Molecular structure of (a) P3HT, (b) MEH-PPV, and (c) MDMO-PPV

B. Synthesis

Ambient Pressure Injection Chemical Vapor Deposition

For this investigation, MWNTs were synthesized using an injection chemical vapor deposition (CVD) process at ambient temperatures. The process, developed in-house at the NanoPower Research Laboratories, was modeled after work at the NASA Glenn Research Center [25]. A picture of the reactor is shown in Figure 6 and a schematic in Figure 7. Initially, argon was selected as the carrier gas and

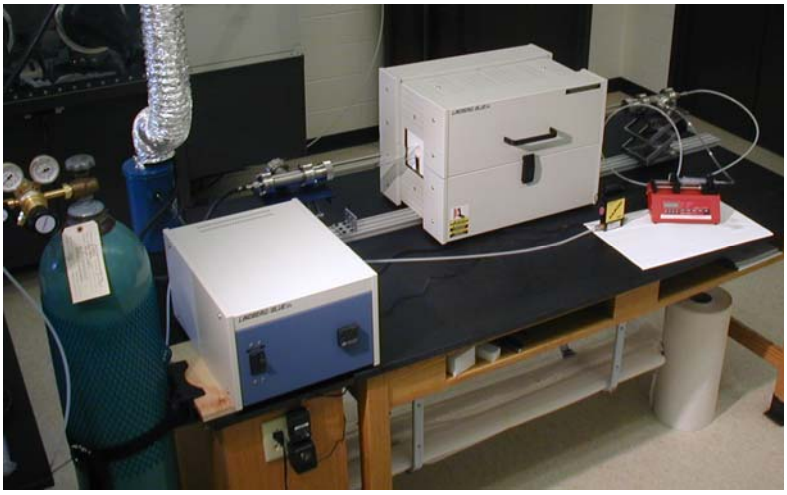

Figure 6. CVD reactor, showing furnace, mechanical syringe pump, and gas flow controller.

cyclopentadienyliron dicarbonyl dimer in toluene was selected as the precursor solution, which was consistent with the group at NASA[25]. Later investigations proved xylene to be a preferable solvent and replaced toluene in the process. A syringe pump was employed to ensure consistent, uniform precursor injection. A

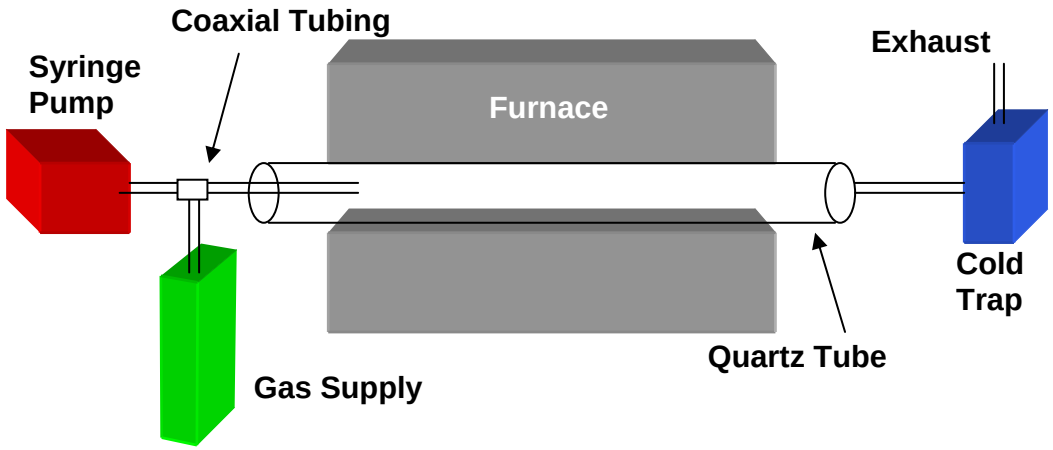

Figure 7. Schematic of CVD reactor. A mechanical syringe pump injects into a coaxial tubing along with a gas supply flow. The stream is carried into the furnace where the produced material collects on the quartz tube. The flow continues down stream to a trap where solid waste is separated from gaseous waste, which exits through the exhaust.

unique coaxial tip was designed for this reactor (Figure 8), where the precursor traveled within a quartz capillary tube that was jacketed by a stainless steel tube that acted as a pathway for the carrier gas. At the tip, the carrier gas was able to aerosolize the precursor and carry it into the furnace. A 2^k design of experiment (DOE) was carried out after the construction of the CVD reactor with five parameters varied as high/low. The temperature, carrier gas flow, precursor concentration, precursor injection rate, and tip injection position were investigated to find optimal parameters for this set-up. Analysis of the DOE results suggested a temperature range from 725 to 800 °C, a gas flow rate of 1.00 L/min, a precursor concentration of 0.08 M, an injection rate of 3.5 mL/hr, and a tip position of 2.5 cm inside the furnace. Material was collected from the interior of the quartz tube within the furnace zone. Investigations were extended to explore the growth of aligned MWNTs. A set of experiments showed it was possible to grow aligned arrays of MWNTs on SiO_2

substrates using the same process parameters as described above. An SEM image of the array on the SiO_2 substrate is depicted in Figure 9.

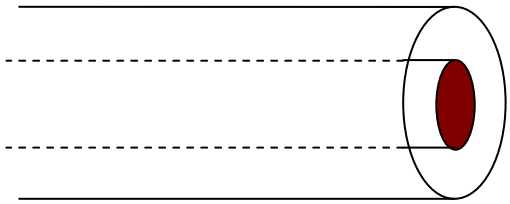

Figure 8. Schematic of coaxial injection tip. Inner capillary tubing carries liquid precursor into furnace and the outer stainless steel tubing acts as a jacket to transport the carrier gas.

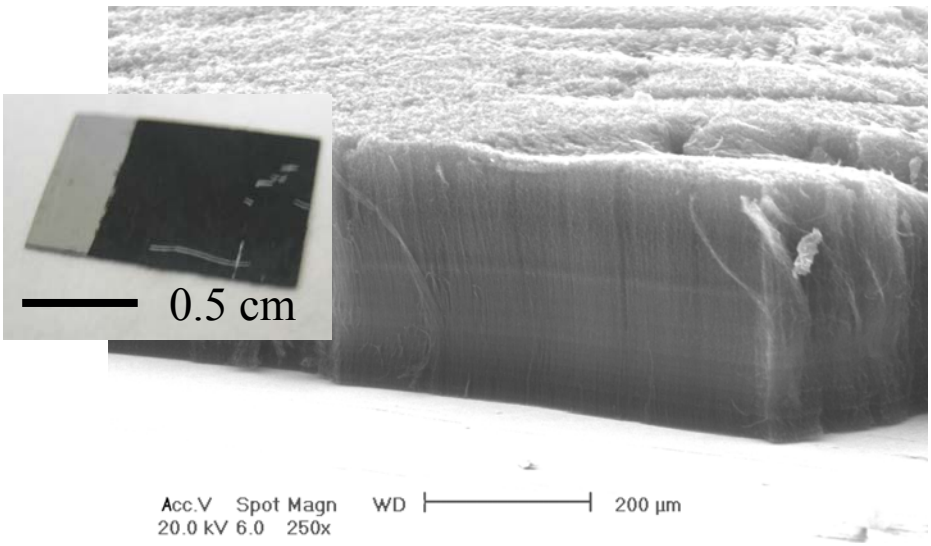

Figure 9. SEM image of aligned MWNT array on SiO_2 substrate with photograph of substrate on left.

B. Characterization

Carbon nanotubes are a novel inclusion into several energy storage and conversion devices due to their unique electrical and mechanical properties. A complete understanding of their material properties is necessary to ensure effective use of carbon nanotubes in a variety of applications. This section explores the commonly used instruments for MWNT characterization and their utility in MWNT research. A spectrum of techniques can be used to effectively characterize MWNT quality and purity including spectroscopy, microscopy, and thermal analysis techniques.

Spectroscopy

Raman Spectroscopy

Raman spectroscopy is a technique used to observe symmetric vibrations in a sample at a particular excitation wavelength. The electrons within the sample are promoted to an excited electronic state and relax to a vibrational state, followed by a recombination to the ground state. The energy difference between the excitation energy and the emitted light is the Raman shift (cm^{-1}). These shifts relate to specific peaks for the vibrational modes of a given sample. For MWNTs, there are three commonly observed peaks, the D-band, G-band, and G'-band (Figure 10). Defects or sp^3 bonding give rise to the D-band; the G-band arises from the graphitic nature or sp^2 bonding of the carbon and this peak is common to many carbon species. The third

peak is the G'-band, which is a result of long range order in the sample which allows for resonance processes[17].

For this work, Raman spectroscopy was performed using a JY-Horiba Labram spectrophotometer at room temperature with excitation energies of 1.96 and 2.54 eV. Sample spectra were taken from 100 – 3000 cm^{-1}.

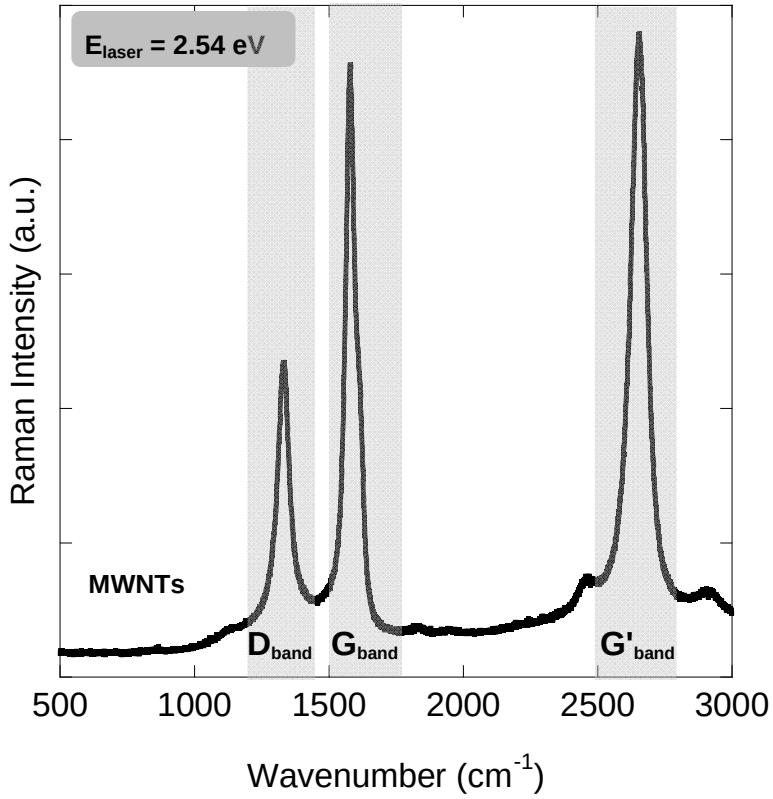

Figure 10. Raman spectra of MWNTs, taken with a 2.54 eV excitation energy, shows the three common bands of MWNT samples: D band, G band, and G' band.

Microscopy

Scanning Electron Microscopy (SEM)

Scanning electron microscopy is a technique in which scattered electrons from a sample are detected to evaluate the sample surface morphology. This technique can provide qualitative measurements of quality for a sample by showing coatings, metal catalyst particles, and bundling of tubes in a sample. Figure 11 shows an SEM image of (a) as-produced MWNTs and (b) nanostructured carbon, both observable with an SEM in a given nanotube sample. Outer diameter measurements for MWNTs are possible with this technique as well. With a large sample set, an outer diameter distribution is possible.

For this work, a Hitachi S-900 near-field emission instrument was used. Samples were prepared on a stub by either carbon tape or silver paint adhesion. The instrument was operated at an accelerating voltage of 2 kV and image magnifications ranged from 5 – 100 kX.

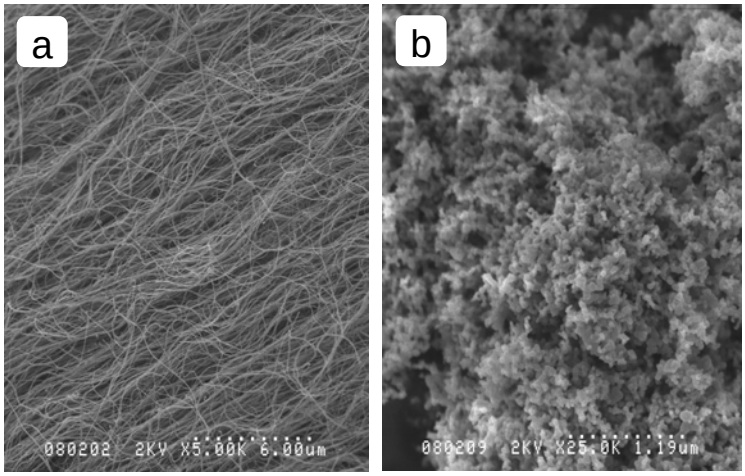

Figure 11. SEM image of (a) as-produced MWNTs and (b) nanostructured carbon

Transmission Electron Microscopy (TEM)

Transmission electron microscopy is a technique in which electrons are passed through a sample to observe its atomic arrangement. In the case of MWNTs, TEM is a practical tool because it allows for the confirmation of multiple walls and the counting of those walls in a MWNT sample. The observation of carbonaceous coatings on MWNTs and metal catalyst particles is also possible. Diameter distribution measurements are also possible given a large enough sample set is taken. These capabilities allow for a qualitative measurement of purity for samples by confirming the presence of MWNTs, and the relative amounts of carbonaceous species and metal particles. TEM images for this work were acquired in collaboration with NASA Glenn Research Center. A Philips CM200 instrument operated at an accelerating voltage of 200 kV was used. The samples were prepared on carbon grids by depositing material from an acetone suspension on the grid.

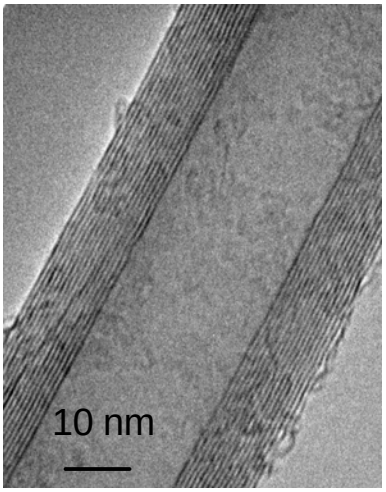

Figure 12. TEM image of a MWNT. Interlayer spacing, as well as inner and outer diameter are observable.

Thermal Analysis

Thermogravimetric Analysis

The technique of thermogravimetric analysis (TGA) provides a quantitative value for the metal composition of a sample. This technique monitors the mass of a sample during thermal decomposition as the sample is ramped to a temperature with a specified rate. Evaluation of the sample decomposition temperatures and the metal residue can lead to quantitative values for purity assessment (Figure 13). Due to the difficulty associated with the convolved decomposition peaks in a typical TGA graph, this technique is not exclusively used to determine purity of MWNT samples. The TGA instrument used in conjunction with other techniques to determine purity for this work was a TA Instruments Model 2950. Samples of ~ 1mg were placed in a platinum pan and ramped at 10 °C/min from room temperature to 1000 °C under air and nitrogen at flow rates of 60 cm^3/min and 40 cm^3/min, respectively.

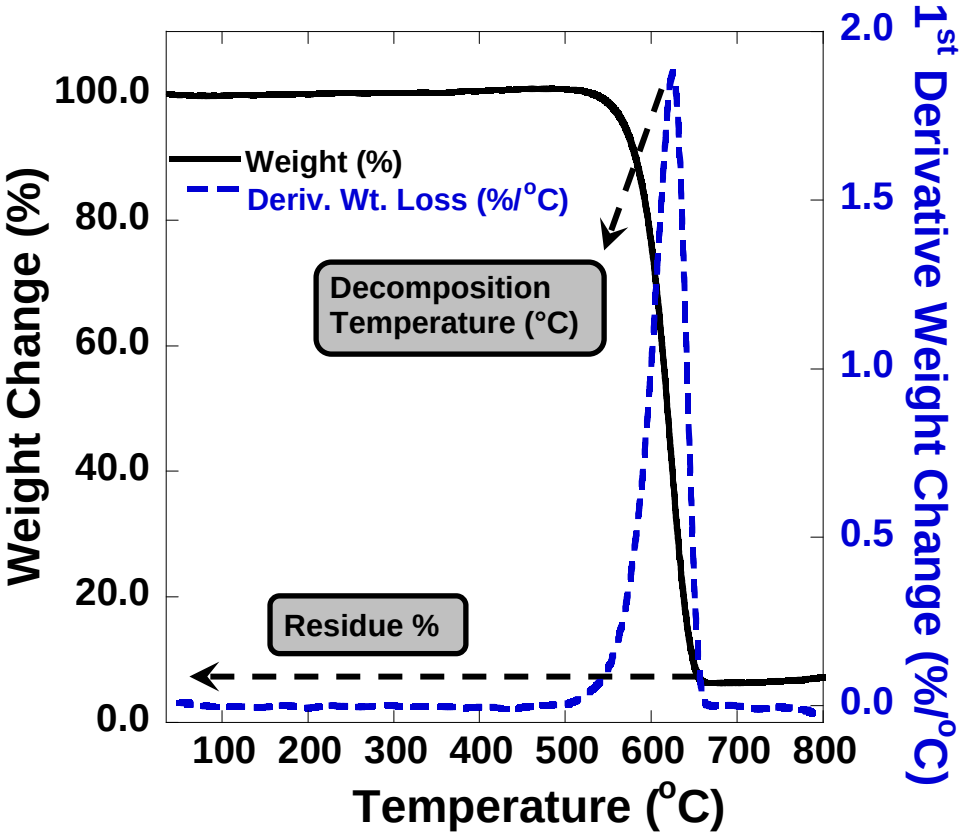

Figure 13. Thermogram of MWNT sample. This can be used to determine the decomposition temperature and percent residue for a sample.

C. MWNT Purity Assessment

APPENDIX A Summary

Purity Assessment of Multi-walled Carbon Nanotubes by Raman Spectroscopy

Roberta A. DiLeo, Brian J. Landi, Ryne P. Raffaelle

J. of Appl. Phys. **2007**, 101, 064307 (2007). Copyright 2007, American Institute of Physics

This publication investigated the utility of Raman spectroscopy, coupled with thermogravimetric analysis and microscopy techniques, to develop a quantitative purity assessment method for MWNTs. The current state of the field lacked a universal, quantitative method of purity assessment for MWNTs. A constructed sample set was prepared from nanostructured carbon and high quality MWNTs to quantify the ratios of the Raman I_D/I_G, $I_{G'}/I_G$, and $I_{G'}/I_D$. From these ratios, calibration curves were developed, and three equations of purity were established. The purities of samples synthesized under various conditions were determined using the established equations of purity. The effectiveness of Raman spectroscopy to provide a quantitative value of purity in combination with thermogravimetric analysis and microscopy techniques was explored.

APPENDIX B Summary

Application of the G'/D Raman Ratio for Purity Assessment of Multi-walled Carbon Nanotubes

Roberta A. DiLeo, Brian J. Landi, Ryne P. Raffaelle

Mater. Res. Soc. Symp. Proc., San Fransisco, California **2007**

Applications of Nanotubes and Nanowires MRS Proceedings San Francisco, CA 2007

Editors: L. Chen and M. Hersam

Mater. Res. Soc. Symp. Proc., **Volume 1081E**, Warrendale, PA 2007 (1018-EE05-11)

This publication extends the investigation of MWNT purity assessment by Raman spectroscopy, coupled with thermogravimetric analysis and scanning electron microscopy, to a second excitation energy. The initial work was completed using an excitation energy of 2.54 eV, while the investigation was furthered by exploring the use of an excitation energy of 1.96 eV. Similar to the previous work, equations of purity were established based upon the Raman ratios, I_D/I_G, $I_{G'}/I_G$, and $I_{G'}/I_D$, and employed to determine purities of a variety of samples, including a sample of aligned MWNTs on SiO_2. An excitation-energy dependent shift was observed for the D and the G' bands of the Raman spectra, whereas the G band remained unshifted. MWNTs show a high sensitivity for the $I_{G'}/I_D$ ratio, and one equation of purity can be applied universally for this ratio across both excitation energies.

A. Material Characterization

Cyclic voltammetry is a characterization technique that offers the capabilities of probing important electronic material properties. In order to eliminate costly device fabrication to test material compatibility, the technique of cyclic voltammetry was employed to quickly determine energy levels of commonly used materials in organic photovoltaics. The characterization of these materials acts as a baseline of comparison for the incorporation of new materials. With cyclic voltammetry,

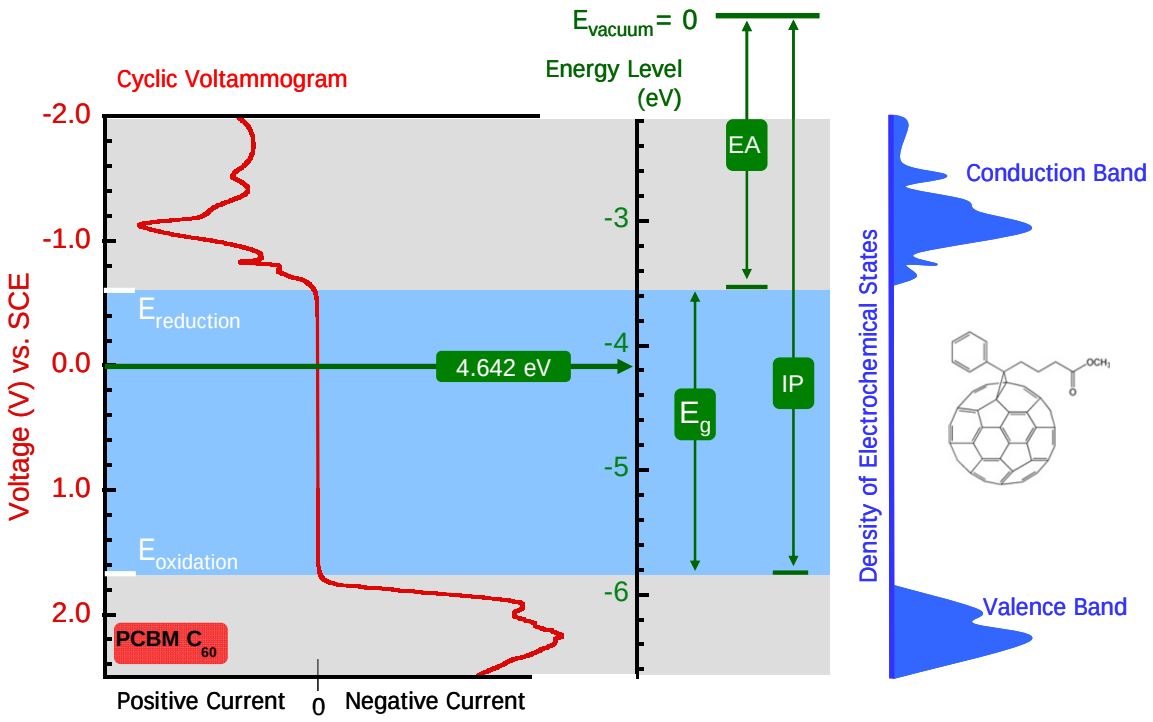

Figure 14. Diagram depicting the use of a voltammogram to extract electronic properties of a sample. The reduction and oxidation potentials are used to calculate the electron affinity (EA) and ionization potential (IP) for a given sample using the reference electrode (in this case standard calomel electrode) and also the band gap by finding the difference between the EA and IP.

ionization potentials (IP) and electron affinities (EA), may be calculated, which correspond to valence states and conduction states, respectively. The band gap (E_g) can be obtained by taking the energy difference of the EA and IP. Electrochemical measurements determine the reduction-oxidation potentials of a material by measuring the voltages at which a material reduces or oxides with respect to a reference electrode. These reduction-oxidation potentials can be used to calculate the electron affinity and ionization potential of a material as explained by Kucur[26]:

$$EA = -(E_{red} + \Delta E_{electrode,vacuum}) \quad (1)$$

$$IP = -(E_{ox} + \Delta E_{vacuum,electrode}) \quad (2)$$

Cyclic voltammetry is also a beneficial technique in regards to photovoltaic fabrication because it eliminates some costly and time consuming processing. From the pertinent information gathered from a typical voltammogram (Figure 14), proper material selection can be made based upon EA, IP, and E_g. As Figure 14 shows, these three values are easily discernable from the voltammograms.

Cyclic voltammetry measurements were taken for a myriad of samples. All measurements were taken with an electrochemical analyzer from CH Instruments using a platinum rotating disk electrode, a platinum wire auxiliary electrode, and a KCl saturated standard calomel electrode (SCE) as the reference electrode within a dark box to control illumination effects (Figure 15). The electrolyte, tetrabutylammonium hexafluorophosphate ($TBAPF_6$) in acetonitrile, 0.1 M, was selected due to its large window of stability and generally nonreactive interaction

with samples. Argon gas was passed through the three-neck electrochemical cell both before and during sample measurements. A scan rate of 20 mV/s was applied while select samples were rotated between 50-100 rpm for laminar flow across the electrode surface. For the illumination studies the samples were illuminated with a halogen lamp (λ_{max} = 630) and a UV lamp (λ_{max} = 350).

A Perkin Elmer Lambda 900 was used to take optical absorption measurements. An acquisition range of 300 to 2000 nm was used to identify maximum absorption peaks which were correlated with band gaps calculated from the voltammograms.

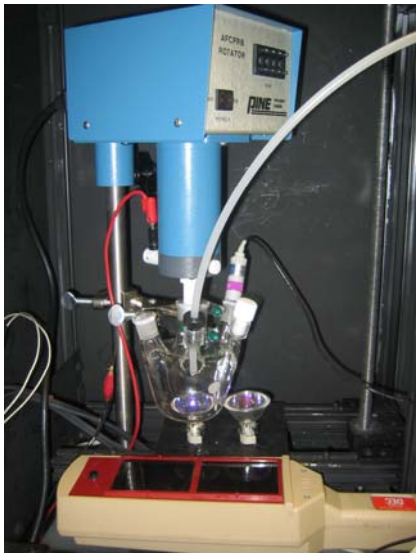

Figure 15. 3-neck cell holding the rotating disk electrode, reference electrode, and counter electrode and the gas input inside the black box.

B. Quantum Dots and Fullerene Derivatives

A colloidal synthesis method was employed for the quantum dots used in this work. For the CdSe quantum dots, a similar procedure was followed in previous reports[27]. A CdO precursor was used, and after nucleation and growth, the dots

were extracted with a methanol: hexane mixture (Figure 16). The trioctylphosphine oxide (TOPO) capped dots underwent a ligand exchange with pyridine, using centrifugation at 6000 rpm for 10 minutes and sonication. UV-Vis-NIR spectroscopy and fluorescence was used to verify the band gap of the quantum dots. Samples are shown in Figure 16.

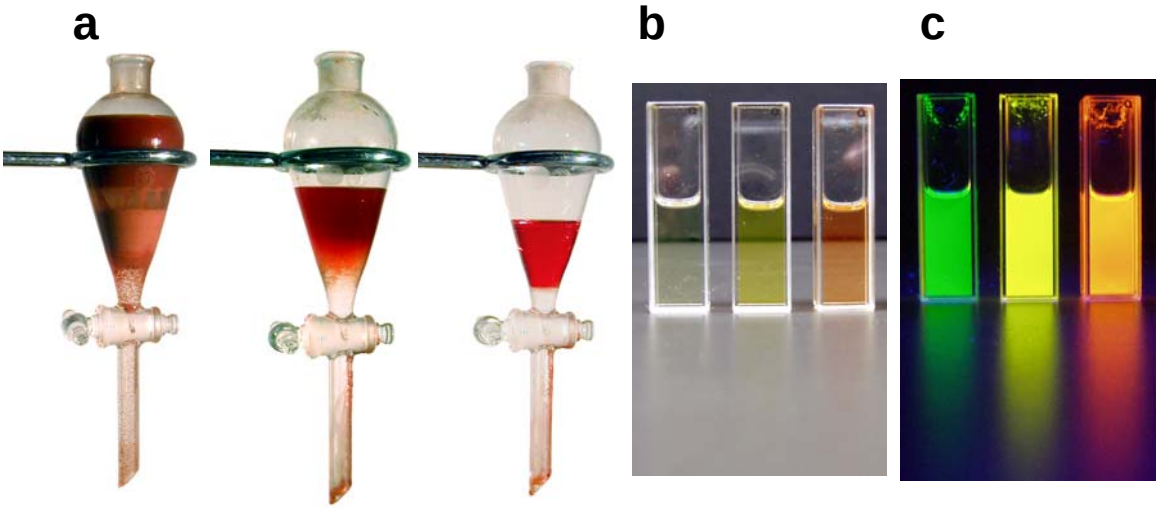

Figure 16. (a) Quantum dot methanol/hexane extraction/cleaning process steps for 3.31 nm CdSe quantum dot, (b) three sizes (3.08, 2.56, and 2.30 nm) of cleaned quantum dots, and (c) three sizes (3.08, 2.56, and 2.30 nm) of dots fluorescing

APPENDIX C Summary

Determination of Nanomaterial Energy Levels for Organic Photovoltaics by Cyclic Voltammetry

Roberta A. DiLeo, Annick Anctil, Cory D. Cress, Brian J. Landi, and Ryne P. Raffaelle

Nanostructured Solar Cells MRS Proceedings Boston, MA 2007

Editors: Antonio Luque and Antonio Marti

Mater. Res. Soc. Symp. Proc., **Volume 1031E**, Warrendale, PA, 2007 (1031-H09-54)

This publication explores the electronic properties, in particular energy level alignment, of a variety of materials commonly used in organic photovoltaics. Specific highlights include: CdSe quantum dots and the shifts that occur in their IP and EA due to changes in dot size; a series of fullerene derivatives that vary in both size and substituent groups; and polymer composites examined in isolation and under illumination. For CdSe quantum dots for a range of diameters, shifts occur in both the IP and EA; however, the degree of shift varies depending on the measurements taken at the peak maximum point or at the peak onset point. The fullerene series investigation showed that energy levels shift with a change in fullerene cage size as well as with the addition of certain substituent groups. A polymer composite of MEH-PPV: PCBM C_{60} was selected for investigating the effects of illumination on energy levels. Initially, voltammograms were measured for each of the components

of the composite, followed by measuring the composite. Finally, the composite was measured both in the dark and under illumination. This series of measurements was useful for understanding the interactions that occur within the composite, where charge transfer occurs, and how these interactions affect the detectable energy levels. Also the illumination studies gave insight as to how the composites will behave in a practical versus laboratory setting.

C. Polymers

Cyclic voltammetry was performed on each of the three commonly used polymers, MEH-PPV (PolySemi), P3HT (Poly(3-hexylthiophene-2,5-diyl)) and MDMO-PPV (Poly[2-methoxy-5-(3′,7′-dimethyloctyloxy)-1,4-phenylenevinylene]) (all purchased from Sigma-Aldrich, in isolation). From the voltammograms (Figure 17), the oxidation and reduction potentials were determined for each polymer. These were considered the baseline to which other nanomaterials and composites were compared.

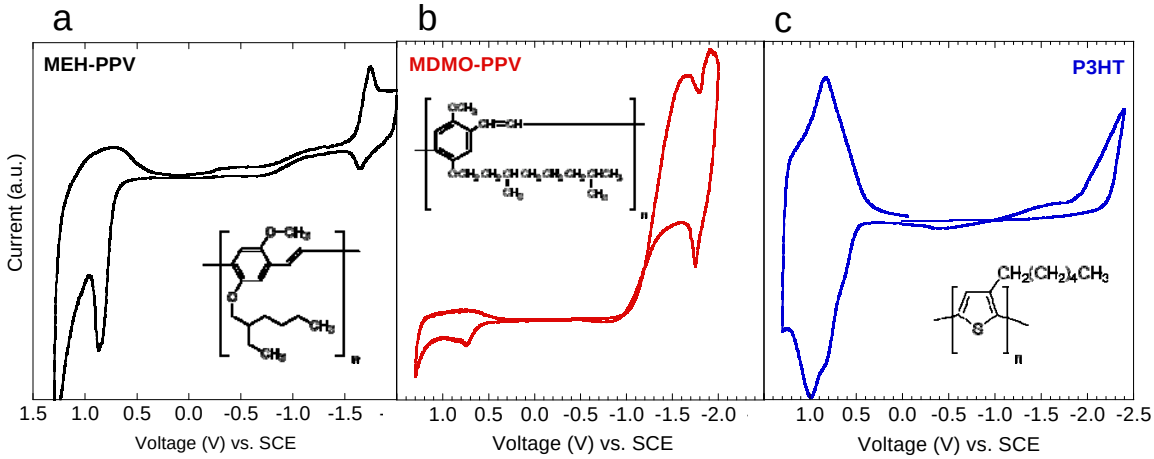

Figure 17. Voltammograms of (a) MEH-PPV, (b) MDMO-PPV, and (c) P3HT with molecular structures as insets for each.

To determine if a shift in energy levels is results from a molecular weight influence, three molecular weight ranges of MEH-PPV were investigated (M_n = 40,000 – 70,000, M_n = 70,000- 100,000, M_n = 150,000 – 250,000). Their voltammograms are shown in Figure 18. There is a clear shift to larger values in the oxidation potential at

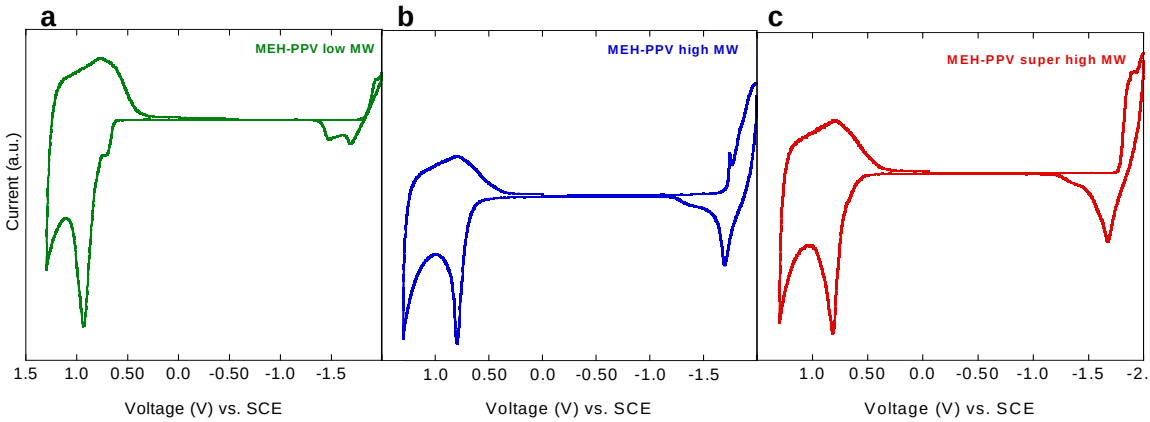

Figure 18. Voltammograms of (a) low MW of MEH-PPV, (b) high MW of MEH-PPV and (c) highest MW of MEH-PPV.

lower molecular weight (Figure 18a). A third subset of polymers was also investigated. These consisted of polymers which have similar structures to the MEH-PPV, but have different structures on the end of the polymer chains, labeled at Polymer 100E and 200E (purchased from American Dye Source). Figure 19 (inset of polymer structure) shows the voltammograms of these polymer derivatives and the clear change in reduction-oxidation potentials due to the change in molecular structure of the polymers.

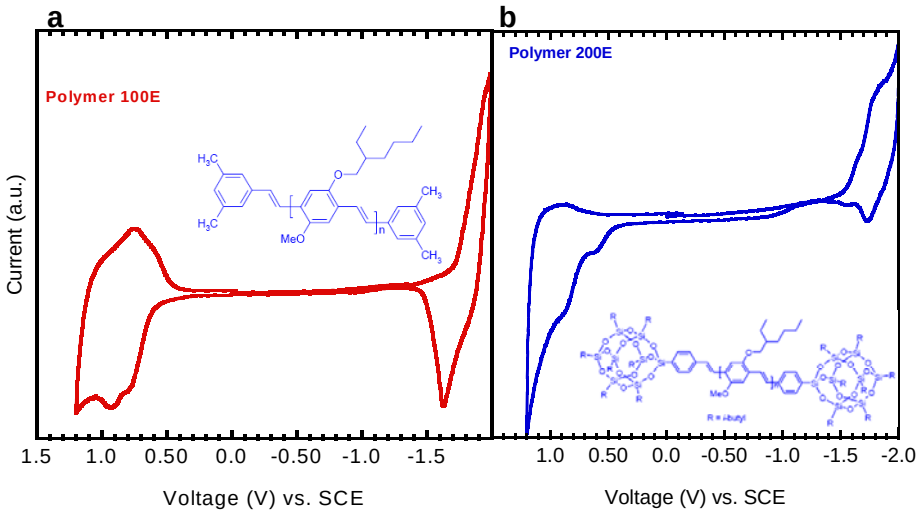

Figure 19. Voltammograms of two PPV polymer derivatives (a) polymer 100 E and (b) 200 E with molecular structure as an inset for each

D. Composites

A comprehensive understanding of energy level alignment was developed from comparing the collective observations from all the materials tested in isolation with the composites that were also investigated. Figure 20 shows the voltammograms of three composites. The resulting curve for a composite is not a simple superposition of the two curves of the components for that given composite. Both curves are resembled, but with shifting in some energy levels and with the assimilation of others. These curves provide insight into the materials' electronic interaction and properties, such as charge transfer in the composite.

Along with testing the composites, scans were completed in the dark and under illumination for the composites Figure 20 shows the voltammograms of the dark and illuminated composites, which is representative of an environment that the composites would be operating in. The composites were illuminated with a halogen bulb and a UV lamp. Small shifts in the reduction-oxidation potentials are visible, with the largest seen in the oxidation potential of the MEH-PPV: PCBM C_{60} composite (Figure 20a). While there are noticeable changes in current intensity while the sample is being illuminated, this work does not discuss the cause of that phenomenon, which could be related to available states for filling.

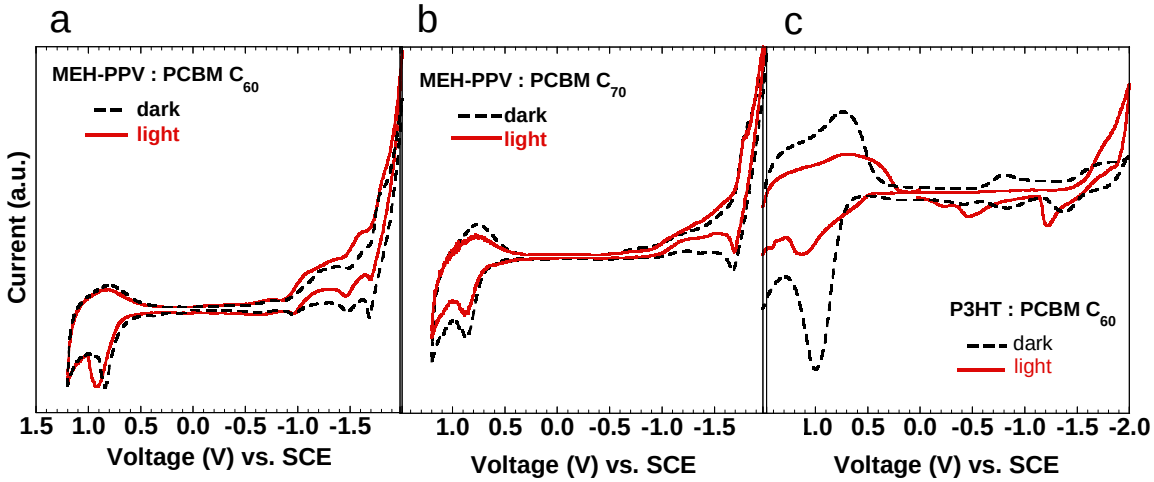

Figure 20. Voltammograms of composites under both dark conditions (black-dotted curves) and under illumination (red curves) (a) MEH-PPV: PCBM C_{60}, (b) MEH-PPV: PCBM C_{70}, (c) P3HT: PCBM C_{60}.

CHAPTER 4 CONCLUSIONS

The focus of this work has been the development of an understanding of material synthesis and characterization for energy conversion and storage devices. A portion of this work has been dedicated to the synthesis and purity assessment of MWNTs for incorporation in device applications, and required an investigation of synthesis conditions to optimize material yield and quality. To further quantify the quality of the as-produced material, a quantitative purity assessment method was developed based upon Raman spectra of the samples. Equations of purity were extracted from the Raman ratios and purity values were assigned to a variety of MWNT samples. The work was extended to include a second excitation energy (2.54 eV and 1.96 eV) to improve the utility of the assessment method. One equation of purity developed from the $I_{G'}/I_D$ band could be used universally for the two excitation energies. After the synthesis optimization, the growth of aligned MWNT arrays was possible on SiO_2 substrates using the typical synthesis conditions. The utility of the purity assessment method was further developed to assess the purity of the aligned MWNT arrays.

Another aspect of this work focused on synthesis and characterization of materials pertinent in organic photovoltaic fabrication, which included semi-conducting quantum dots, fullerene derivatives, and polymers. A series of CdSe quantum dots were synthesized and characterized to determine changes in band gap and shifts in the EA and IP in conjunction with the changing band gap. A set of four different sizes of quantum dots spanning a band gap of 2.2 eV to 2.48 eV resulted in observable shifts in both the EA and IP in the cyclic voltammogram. A second nanomaterial, the

fullerene derivative PCBM C_{60}, was characterized. This lead to an investigation of a series of fullerene derivatives, which included the PCBM C_{60}, PCBM C_{70}, PCBA C_{60} and ThCBM C_{60}. There were observable shifts in the IP of the four derivatives as well as shifts of the EAs and an increase or decrease in the number of measureable energy levels beyond the EA for each derivative. Electrochemical measurements of three commonly used polymers in isolation were performed. Polymers act as the starting material to which nanomaterials are added. By characterizing the polymers as well, a fuller understanding can be gained for interactions that occur within the

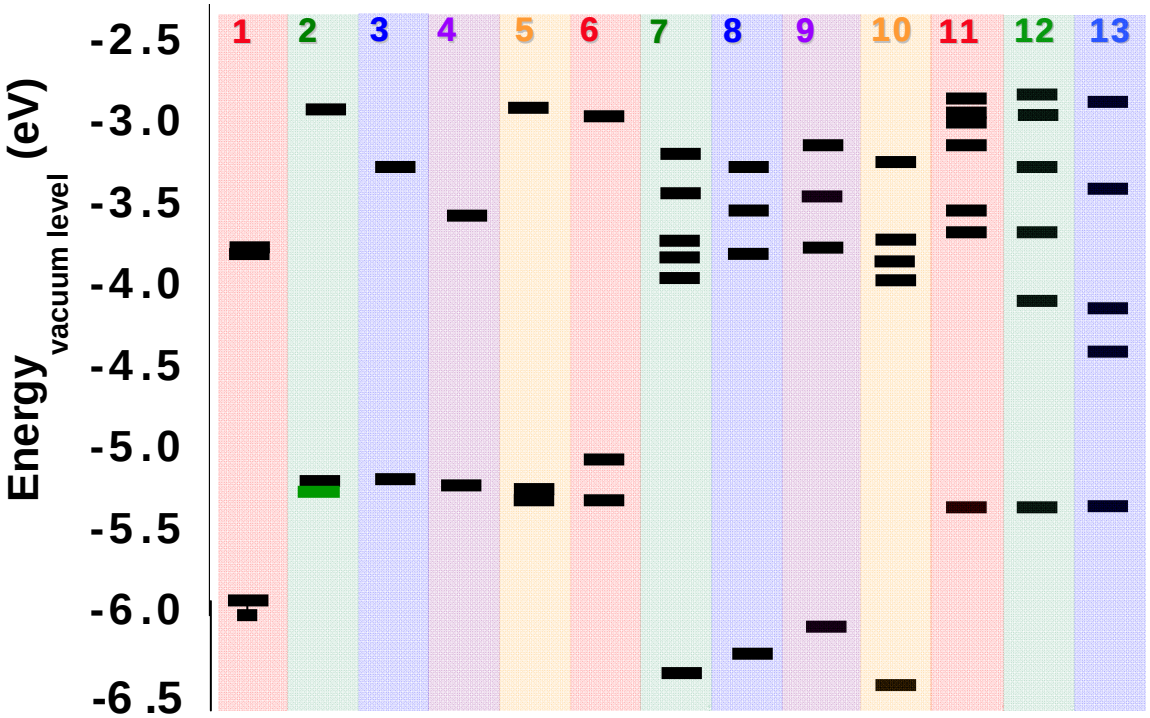

Figure 21. Energy level diagram for all the materials which were examined using the technique of cyclic voltammetry during this work: (1) CdSe QD's shifts in EA and IP designated by double-line, (2) MEH-PPV- second IP designates MW influenced shifts, (3) P3HT, (4) MDMO-PPV, (5) Polymer 100E, (6) Polymer 200E, (7) PCBM C_{60}, (8) PCBM C_{70}, (9) PCBA C_{60}, (10) ThCBM C_{60}, (11) MEH-PPV: PCBM C_{60}, (12) MEH-PPV : PCBM C_{70}, and (13) P3HT: PCBM C_{60}.

composite.

The energy level diagram in Figure 21 shows the expanse of the materials investigated through electrochemical characterization. This diagram is also useful in pre-selecting materials for device design and fabrication due to the ability to visually check the compatibility of energy levels for any combination of materials. The diagram confirms the changes observed in the energy levels of the composites versus those of the materials in isolation. The information gathered by electrochemical characterization also aids in the understanding of device performance by correlating material energy properties with devices properties such as open-circuit voltage, short circuit current, fill-factor, and efficiency.

This work contributes overall to the forward progress of the field of energy storage and conversion devices by the development and characterization of new materials which is vital to the growth of this technological field. The proper combination of materials is essential for all of the devices that fall under this heading, whether it is due to energetic properties, weight, volume capacity or a variety of other restrictions. The results of this work, in particular the methods of characterization, will have a lasting impact on the material selection for future device fabrication in the field of energy storage and conversion.

APPENDIX A: *Purity Assessment of Multiwalled carbon nanotubes by Raman Spectroscopy* (*J. of Appl. Phys.* **2007**, 101, 064307) Reprint permission from American Institute of Physics

JOURNAL OF APPLIED PHYSICS **101**, 064307 (2007)

Purity assessment of multiwalled carbon nanotubes by Raman spectroscopy

Roberta A. DiLeo
Department of Physics, Rochester Institute of Technology, Rochester, New York 14623 and NanoPower Research Laboratories (NPRL), Rochester Institute of Technology, Rochester, New York 14623

Brian J. Landi
NanoPower Research Laboratories (NPRL), Rochester Institute of Technology, Rochester, New York 14623

Ryne P. Raffaelle[a)]
Department of Physics, Rochester Institute of Technology, Rochester, New York 14623 and NanoPower Research Laboratories (NPRL), Rochester Institute of Technology, Rochester, New York 14623

(Received 8 December 2006; accepted 19 January 2007; published online 22 March 2007)

Carbonaceous purity assessment for chemical vapor deposition multiwalled carbon nanotubes (MWNTs) using Raman spectroscopy was investigated. Raman spectroscopy was performed on a reference sample set containing predetermined ratios of MWNTs and representative synthesis by-products. Changes in the characteristic Raman peak ratios (i.e., I_D/I_G, $I_{G'}/I_G$, and $I_{G'}/I_D$) as a function of MWNT content were measured. Calibration curves were generated from the reference samples and used to evaluate MWNTs synthesized under different conditions with varying purity. The efficacy of using Raman spectroscopy in conjunction with thermogravimetric analysis for quantitative MWNT purity assessment is discussed. © *2007 American Institute of Physics*.
[DOI: 10.1063/1.2712152]

I. INTRODUCTION

Since the discovery of multiwalled carbon nanotubes (MWNTs),[1] researchers have investigated their use in various applications due to their remarkable electrical, mechanical, and chemical properties.[2–5] MWNTs share many of the same attributes of a single walled carbon nanotube (SWNT) but may offer a greater potential for low-cost production. Recent advancements of MWNTs have been due to improved bulk synthesis (i.e., high quality materials) and their potential in power devices.[2] MWNT synthesis can be achieved through an array of methods involving the catalytic decomposition of carbon containing compounds.[2] However, each synthesis technique results in a mixture of MWNT structures with impurities (i.e., metal catalyst and carbonaceous materials). Therefore, a simple method to quantify MWNT purity, similar to that of SWNTs, is desirable.[6]

Several qualitative and quantitative techniques have been used to characterize MWNT samples, including scanning electron microscopy (SEM), transmission electron microscopy (TEM), thermogravimetric analysis (TGA), and Raman spectroscopy.[7–12] However, the proper combination of these techniques (or others) to produce a protocol for quantifying MWNT purity (defined as the mass fraction of nanotubes in a sample) has yet to be established. Commonly used microscopy can be quite useful at quantifying nanotube diameter or interlayer spacing. However, these methods provide a qualitative understanding of the MWNT purity as they are limited in their ability to determine other factors affecting purity (e.g., degree of carbonaceous coatings, encapsulated metal particles, etc.). While TGA can accurately quantify a sample's metal content, the decomposition curve cannot easily be deconvolved to provide carbonaceous MWNT purity. Attempts to use Raman spectroscopy for purity assessment have relied upon a ratio of the *D*-band peak (~1350 cm^{-1}) and the *G*-band peak (~1580 cm^{-1}) to infer a purity level. However, with no reference for comparison, ambiguity arises in the interpretation of data for these two peaks due to the effects that carbon impurities have on the bands' intensities. Therefore, a ratio containing the *G′*-band peak (~2700 cm^{-1}) may represent a more accurate measurement of MWNT quality or purity, since the *G′* band resonant Raman intensity is dramatically enhanced in the case of carbon nanotubes.[13]

In the present work, a method of using Raman spectroscopy to assess MWNT purity is developed as a complement to SEM, TEM, and TGA. Along with the appropriate characterization techniques, there exists a concomitant necessity to identify a reference sample or a constructed calibration set for MWNT purity verification. The use of a constructed sample set to develop the necessary reference is analogous to previous work on the purity assessment of SWNTs.[6] A constructed sample set consists of samples with varying concentrations of a reference MWNT sample (relative 100% MWNT) and a representative carbonaceous impurity (0% MWNT). Trends in the Raman spectra of the constructed sample set, which vary monotonically with sample purity, were investigated, and evaluation of the Raman peak ratios

a)Electronic mail: rprsps@rit.edu

 © 2007 American Institute of Physics

Downloaded 23 Mar 2007 to 129.21.157.70. Redistribution subject to AIP license or copyright, see http://jap.aip.org/jap/copyright.jsp

APPENDIX A: *Purity Assessment of Multiwalled carbon nanotubes by Raman Spectroscopy* (*J. of Appl. Phys.* **2007**, 101, 064307) Reprint permission from American Institute of Physics

for samples synthesized under a factor screening experiment shows a good correlation with qualitative estimations based on their SEM images.

II. EXPERIMENT

The MWNTs used in this work were synthesized using a procedure similar to those previously reported.[2,14] In short, an injection chemical vapor deposition (CVD) reactor was constructed with a coaxial injection design. The injection tip was fabricated using quartz capillary tubing (i.d. 1 mm, o.d. 3 mm) encased in a stainless steel jacket. In the factor screening experiment, temperature and precursor concentration (cyclopentadienyl iron dicarbonyl dimer in toluene) were varied. Material was synthesized at temperatures of 725 and 875 °C, precursor concentrations of 0.04*M* and 0.08*M*, a gas flow rate of 0.75 l/min, and a precursor delivery rate of 3.5 ml/h. Field emission SEM was performed for MWNT samples using a Hitachi S-900 instrument. TGA was performed on samples of ~1 mg ramped at 10 °C/min from 25 to 1000 °C under a flow of air at a rate of 60 SCCM (SCCM denotes cubic centimeters per minute at STP) with a TA Instruments 2950. Raman spectroscopy on the factor screening experiment samples and the constructed sample set was performed using a Jobin Yvon LabRam spectrophotometer with an excitation energy of 2.54 eV and an acquisition range from 100 to 3000 cm^{-1}.

For use in the constructed sample set, representative carbonaceous by-products were produced using a similar procedure (injection CVD) but without the inclusion of the organometallic precursor (only toluene was injected). This procedure yielded small amounts of carbonaceous materials which were representative of the by-products produced in the MWNT synthesis as indicated by microscopy and Raman spectroscopy. Because of the low yield, a surrogate, nanostructured carbon was used, which was produced in a laser vaporization process in large quantities. This material was representative of the MWNT CVD synthesis carbonaceous by-products based upon SEM, TGA, and Raman analysis. MWNTs used in the constructed sample set were synthesized at 725 °C, an argon gas flow rate of 0.75 l/min, a precursor injection rate of 3.5 ml/h, and a precursor concentration of 0.08*M*. The constructed sample set was prepared from solutions of varying amounts (100%, 80%, 60%, 40%, 20%, and 0%) w/w of MWNTs mixed with nanostructured carbon in hexanes to produce 0.5 mg/ml solutions. The stock solutions containing the reference 100% MWNTs and 0% MWNTs were sonicated at 20 °C for 1 h, stirred at room temperature for 4 h, and sonicated for 30 min at 20 °C. Each constructed weight percent sample was homogenized using a similar process (1 h sonication at 20 °C, a 4 h stir at room temperature, and a 30 min sonication at 20 °C). Samples were filtered using a 0.02 μm alumina filter. A comparison of the Raman spectra of the as-produced material and the "100%" MWNT sample in hexanes was completed to ensure no damage was incurred during the homogenization-sonication process.

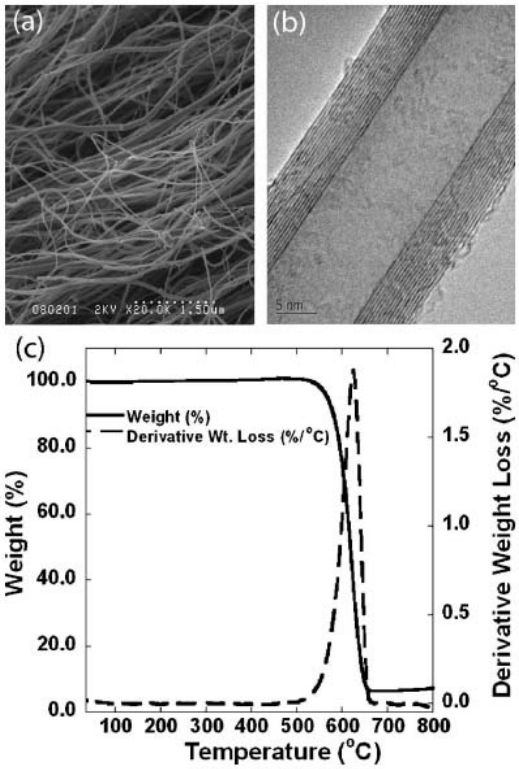

FIG. 1. (a) Field emission SEM image of relative 100% MWNT sample at magnification 20 000x, (b) TEM image of relative 100% MWNT sample showing concentric layers, and (c) TGA thermogram of relative 100% MWNT sample.

III. RESULTS AND DISCUSSION

The selection of a 100% MWNT sample is an important consideration, since a known sample is unavailable. Therefore, this work is based upon the highest purity material synthesized, as measured by SEM, TEM, TGA, and Raman (see Fig. 1). The SEM image is representative of the sample morphology and shows an abundance of nanotubes and little, if any, carbonaceous or metal catalyst impurities. The TEM image confirms that the nanoscale materials seen in the SEM image were indeed tubular and contained multiple concentric cylinders. The TGA thermogram illustrates the decomposition temperature of ~625 °C and the low metal catalyst residue at ~6% by weight, which are better than the typical range of values given in the literature of 550–615 °C and 13%–43%, respectively.[8,10,15,16]

The spectra in Fig. 2(b) show the three characteristic peaks of MWNTs: the *D* band (~1350 cm^{-1}), the *G* band (~1580 cm^{-1}), and the *G′* band (~2700 cm^{-1}). The *D* band is indicative of defects in the MWNT sample (i.e., carbonaceous impurities with sp^3 bonding, broken sp^2 bonds in the sidewalls). The *G* band results from the graphitic nature of the sample (i.e., crystallinity of the sample, pristine arrange-

Downloaded 23 Mar 2007 to 129.21.157.70. Redistribution subject to AIP license or copyright, see http://jap.aip.org/jap/copyright.jsp

APPENDIX A: *Purity Assessment of Multiwalled carbon nanotubes by Raman Spectroscopy* (*J. of Appl. Phys.* **2007**, 101, 064307) Reprint permission from American Institute of Physics

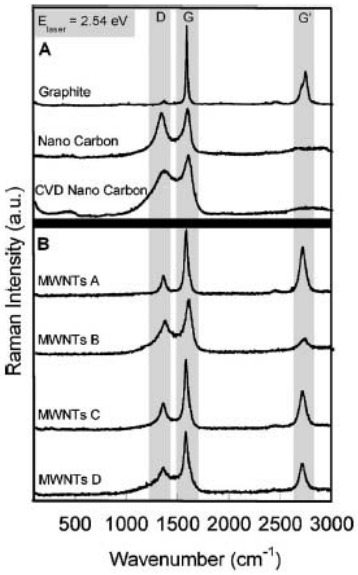

FIG. 2. Overlay of Raman intensity vs wavenumber of CVD nanocarbon, nanocarbon, graphite, and factor screening experiment MWNTs samples at an incident laser energy of 2.54 eV. The *D*, *G*, and *G′* bands, used for the generation of calibration curves, are highlighted and the data are offset for clarity.

ment of atoms), and the *G′* band is indicative of long-range order in a sample and arises from the two-phonon, second-order scattering process that results in the creation of an inelastic phonon.[13]

Several carbonaceous samples were investigated for use as the surrogate carbonaceous by-product in the constructed sample set; Fig. 2(a) depicts the Raman spectra of some of the various species considered. Fig. 2(a) shows the similarities of the Raman spectra of the laser synthesized nanostructured carbon and the nanostructured carbon by-product synthesized in the CVD reactor. The ability to distinguish graphite from MWNTs is another important consideration for a purity assessment method. Figure 2(a) shows that these two materials have similar Raman spectra; however, differences in the *G′* bands can be identified and employed to differentiate between graphite and MWNTs when assessing purity. There is a shift to a higher wavenumber in the peak position of the graphite *G′* band (i.e., from 2715 cm^{-1} in MWNTs to 2738 cm^{-1} in graphite). The presence of graphite can also be corroborated with SEM whereby the graphene sheets are easily discernable at low magnification.

The Raman spectra, normalized to the *G* band peak intensity, of the constructed sample set are shown in Fig. 3. The increase of the *D* band intensity with decreasing MWNT content is a direct result of the addition of carbonaceous by-products. A decrease in the *G′* band intensity as the MWNT mass fraction decreases is also evident. Since the *G′* band results from a two-phonon process it is plausible that its intensity should decrease as the sample becomes less ordered (i.e., more impurities present) not allowing for the coupling

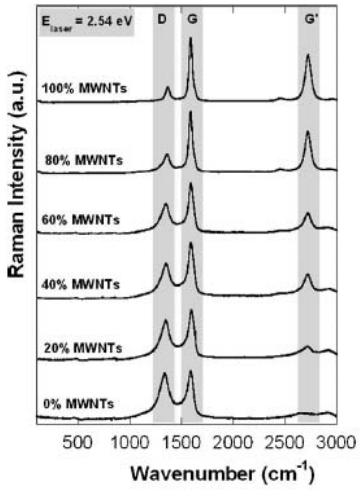

FIG. 3. Raman spectra for constructed sample set composed of MWNTs and nanocarbon at varying weight fractions. The incident laser energy was 2.54 eV. The trends of the *D*, *G*, and *G′* bands can be seen in the highlighted regions, and the data are offset for clarity.

effect which is necessary for the two-phonon process. The relative changes in the various peak intensities clearly correlate with the amount of carbonaceous impurity in a given sample, and it is from this correlation that calibration curves were computed. Relative ratios of the Raman peaks were chosen as opposed to absolute Raman peak intensities since the ratios of peaks are less sensitive to instrument and atmospheric conditions which can cause large changes in absolute intensities.

Three calibration curves were generated from the ratios of the sample set, and the trends followed by each of the Raman ratios (i.e., I_D/I_G, $I_{G'}/I_G$, $I_{G'}/I_D$) are depicted in Fig. 4. This figure shows the linear approximations for the I_D/I_G and $I_{G'}/I_G$ ratios and an exponential approximation for the $I_{G'}/I_D$ ratio. The largest relative change is observed for the $I_{G'}/I_D$ ratio making it the most sensitive to changes in MWNT purity. The equations of the curve fits to calculate the carbonaceous purity of samples are as follows:

$$D/G_{\text{ratio}} = 0.96 - 0.0066X, \quad R^2 = 0.996 \tag{1}$$

$$G'/G_{\text{ratio}} = 0.33 + 0.0045X, \quad R^2 = 0.964 \tag{2}$$

$$G'/D_{\text{ratio}} = 0.31^{*}\exp(0.021X), \quad R^2 = 0.994. \tag{3}$$

where *X* is the purity value.

In order to investigate the applicability of Eqs. (1)–(3), a factor screening study was conducted which utilized experimental parameters (see Table I) to produce MWNT material of unknown and potentially varying purity. As evident from the SEM images in Fig. 5, each of the as-synthesized samples exhibit very different carbonaceous purity, albeit there is no basis to assign quantitative levels. However, using the Raman spectra in Fig. 2(b) and Eqs. (1)–(3), a quantitative comparison of carbonaceous purity can be achieved for

Downloaded 23 Mar 2007 to 129.21.157.70. Redistribution subject to AIP license or copyright, see http://jap.aip.org/jap/copyright.jsp

APPENDIX A: *Purity Assessment of Multiwalled carbon nanotubes by Raman Spectroscopy* (*J. of Appl. Phys.* **2007**, 101, 064307) Reprint permission from American Institute of Physics

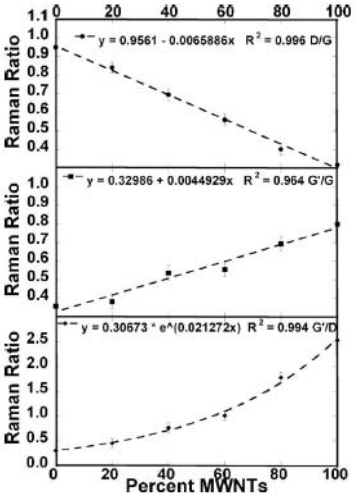

FIG. 4. Data points are the calculated ratios from spectra in Fig. 3. Data were fitted with linear and exponential approximations indicated by the dashed lines. The calibration equations established from the fits are for calculating purity values.

each sample based upon reference to the 100% MWNT sample of the constructed sample set. The calculated values, provided in Table I, correlate very well with the visual SEM evidence of Fig. 5, and thus, support the use of calibration curves from the relative ratios of Raman bands for MWNT purity assessment.

IV. CONCLUSIONS

In conclusion a constructed sample set comprising high purity MWNTs and carbonaceous by-products has been developed to investigate the use of relative Raman ratios for MWNT purity assessment. Calibration curves were established for Raman intensity ratios and the largest relative change was observed in the $I_{G'}/I_D$ ratio. Material was synthesized under varying experimental conditions to produce samples of differing MWNT purity so that the calculated purity based on the three calibration curves could be compared. The calculated MWNT purities derived from the Raman ratios were consistent with SEM observations, demonstrating that the $I_{G'}/I_D$ ratio values showed the smallest deviation to the average purity values. Thus, the use of calibration curves from relative Raman ratios has been demonstrated as a viable means to ascribe reference carbonaceous purity levels. This carbonaceous purity assessment using Raman spectroscopy can be used in concert with conventional metal content analysis from TGA to provide a more comprehensive assessment of the overall MWNT purity in a given sample.

TABLE I. Experimental parameters and purity values from each of the generated calibration curves for the samples of the factor screening experiment.

Sample	Temperature (°C)	Concentration (*M*)	*D*/*G*	*G*′/*G*	*G*′/*D*	Average purity
A	725	0.08	99	93	98	97
B	875	0.08	38	29	35	34
C	725	0.04	71	66	67	68
D	875	0.04	58	59	59	60

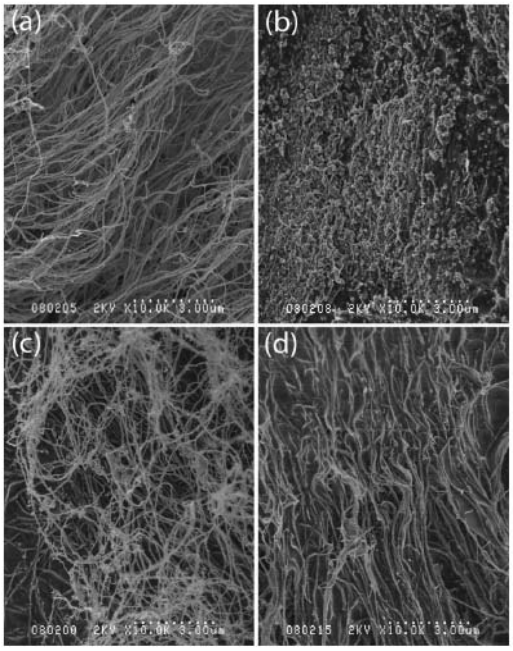

FIG. 5. Field emission SEM images of the four (A, B, C, D) MWNT samples of the factor screening experiment. The magnifications are 10 000x.

ACKNOWLEDGMENT

The authors wish to thank William Van Derveer for his input during this work. Financial support for this project was made by BP Solar, NASA (SUNY Albany, PI Pradeep Haldar) (1046196-2-35652), AFOSR (SUNY Buffalo, PI Paras Prasad) (FA9550-06-0398), NASA (NNC056A60G), and the NRO (RTVGC-05-222). One of the authors (R.A.D.) also acknowledges financial support from the Barry M. Goldwater Scholarship.

[1]S. Iijima, Nature (London) **354**, 56 (1991).
[2]R. P. Raffaelle, B. J. Landi, J. D. Harris, S. G. Bailey, and A. F. Hepp, Mater. Sci. Eng., B **116**, 233 (2005).
[3]M. S. Marcus, J. M. Simmons, O. M. Castellini, R. J. Hamers, and M. A. Eriksson, J. Appl. Phys. **100**, 084306-1 (2006).
[4]Y. Xu, Y. Zhang, E. Suhir, and X. Wang, J. Appl. Phys. **100**, 074302-1 (2006).
[5]G. L. Zhao, D. Bagayoko, and L. Yang, J. Appl. Phys. **99**, 114311-1 (2006).
[6]B. J. Landi, H. J. Ruf, C. M. Evans, C. D. Cress, and R. P. Raffaelle, J. Phys. Chem. B **109**, 9952 (2005).
[7]J. M. Benoit, J. P. Buisson, O. Chauvet, C. Gordon, and S. Lefant, Phys. Rev. B **66**, 073417-1 (2002).

Downloaded 23 Mar 2007 to 129.21.157.70. Redistribution subject to AIP license or copyright, see http://jap.aip.org/jap/copyright.jsp

APPENDIX A: *Purity Assessment of Multiwalled carbon nanotubes by Raman Spectroscopy* (*J. of Appl. Phys.* **2007**, 101, 064307) Reprint permission from American Institute of Physics

[8]W. Huang, Y. Wang, G. Luo, and F. Wei, Carbon **41**, 2585 (2003).
[9]A. M. Keszler, L. Nemes, S. R. Ahmad, and X. Fang, J. Optoelectron. Adv. Mater. **6**, 1269 (2004).
[10]G. S. B. McKee and K. S. Vecchio, J. Phys. Chem. B **110**, 1179 (2005).
[11]R. Murphy, J. N. Coleman, M. Cadek, B. McCarthy, M. Bent, A. Drury, R. C. Barklie, and W. J. Blau, J. Phys. Chem. B **106**, 3087 (2001).
[12]X. Zhao, Y. Ando, L. C. Qin, H. Kataura, Y. Maniwa, and R. Saito, Physica B **323**, 265 (2002).
[13]R. Saito *et al.*, New J. Phys. **5**, 157.1 (2003).
[14]J. D. Harris, R. P. Raffaelle, T. Gennett. B. J. Landi, and A. F. Hepp, Mater. Sci. Eng., B **116**, 369 (2005).
[15]D. Y. Kim, C. Yang, Y. S. Park, K. K. Kim, S. Y. Jeong, J. H. Han, and Y. H. Lee, Chem. Phys. Lett. **413**, 135 (2005).
[16]C. Gommes *et al.*, Colloids Surf., A **241**, 155 (2004).

Downloaded 23 Mar 2007 to 129.21.157.70. Redistribution subject to AIP license or copyright, see http://jap.aip.org/jap/copyright.jsp

APPENDIX B : *Application of the G'/D Raman Ratio for Purity Assessment of Multi-walled Carbon Nanotubes* (MRS Proceedings, San Francisco, California **2007**) Reprint permission from MRS E-Proceedings

Mater. Res. Soc. Symp. Proc. Vol. 1018 © 2007 Materials Research Society 1018-EE05-11

Application of the G'/D Raman Ratio for Purity Assessment of Multi-Walled Carbon Nanotubes

Roberta DiLeo, Brian Landi, and Ryne Raffaelle
Physics, Rochester Institute of Technology, 85 Lomb Memorial Drive, Rochester, NY, 14623

ABSTRACT

Carbonaceous purity assessment methods are being sought after for all types of carbon nanotubes as a means to standardize the material metrology. Our most recent work has evaluated chemical vapor synthesized multi-walled carbon nanotubes (MWNTs). This effort included a protocol for assessment involving qualitative information from scanning electron microscopy (SEM) images and quantitative information from thermogravimetric analysis (TGA) and Raman spectroscopy. Presently, the analysis using Raman spectroscopy on a constructed sample set has been extended to a second excitation energy (HeNe laser at 1.96 eV) and the similar trends in the relative Raman peak ratios have been measured. In contrast to the G-band, the D and G' peaks demonstrate a Raman shift that is excitation energy-dependent, consistent with the double resonance theory. However, the Raman ratio of $I_{G'}/I_D$ is independent of excitation energy and is observed to be the most sensitive to MWNT carbonaceous purity. Application of this approach to MWNT arrays grown on SiO_2 is compared to conventional bulk powders synthesized under similar conditions. The MWNT arrays show a high degree of vertical alignment based upon SEM and a measured carbonaceous purity using the $I_{G'}/I_D$ ratio of 75% w/w.

INTRODUCTION

The discovery of multi-walled carbon nanotubes (MWNTs) over a decade ago[1] has sparked widespread investigations of their unique mechanical, chemical, and electrical properties.[2-5] While MWNTs possess many of the same properties as the closely related single-walled nanotubes, they offer the capability of economical bulk production which leads to further incorporation in power devices.[2] Specifically, aligned MWNT arrays are attractive for building solar cells, sensors, integrated circuits, carbon yarns for macroscopic structures, along with other capabilities.[2,6-8] Many methods of catalytic decomposition of carbon containing compounds are used in the synthesis of MWNTs.[2] Still, with each technique a mixture of MWNTs and impurities (i.e. metal catalyst and carbonaceous materials) is the resulting product. A method of MWNT purity quantification is advantageous because of this resulting mixed product.

While several quantitative and qualitative techniques exist and are used to characterize MWNTs, a method of assessment which combines scanning electron microscopy (SEM), thermogravimetric analysis (TGA) and Raman spectroscopy has recently been reported.[9] Although microscopy offers a simple qualitative verification of purity, TGA and Raman spectroscopy have the capability to evaluate purity with more quantitative results. Our reported method focuses on the use of the Raman peak ratios to determine purity (defined as the mass fraction of nanotubes in a sample) from calibration curves developed from a constructed sample set. Constructed sample sets offer a standard for use in purity evaluations.

APPENDIX B : *Application of the G'/D Raman Ratio for Purity Assessment of Multi-walled Carbon Nanotubes* (MRS Proceedings, San Francisco, California **2007**) Reprint permission from MRS E-Proceedings

In the present work, a second excitation energy was used in the Raman spectroscopy characterization to further investigate the purity assessment method and calibration curves we previously developed. Equivalent trends in the data were noted from the 1.96 eV and the 2.54 eV lasers and the consistency of sample purity determination using the $I_{G'}/I_D$ was investigated. In addition application of this method was extended to MWNT arrays and compared to the results of bulk MWNT powder.

EXPERIMENT

An injection chemical vapor deposition (CVD) reactor was used to synthesize the MWNT aligned arrays in this work similar to procedures previously reported.[9, 10] A precursor delivery rate of 3.5 mL/h, a gas flow rate of 0.75 L/min, a temperature of 725 °C, and a precursor concentration of 0.08 M were employed to synthesize the material on SiO_2. A constructed sample set was prepared according to our previous report. Stock solutions of a relative 100 % and 0 % MWNT solution were mixed to arrive at six samples with varied content (100 %, 80 %, 60 %, 40 %, 20 %, and 0 %) w/w of MWNTs. These solutions were homogenized before filtering. Thermogravimetric analysis was performed on ~ 1 mg samples under conditions of temperature ramping of 10 °C/min from 25 °C -1000 °C with an air flow rate of 60 sccm with a TA Instruments 2950. Scanning electron microscopy (SEM) was performed on the MWNT aligned arrays using a Hitachi S-900 instrument and a Philips XL 30 ESEM instrument. Raman spectroscopy was performed on the constructed sample set along with the MWNT aligned arrays with a Jobin Yvon LabRam spectrophotometer with excitation energies of 2.54 eV and 1.96 eV and an acquisition range of 100-3000 cm^{-1}.

DISCUSSION

Figure 1 shows the Raman spectra from the constructed sample set using a 1.96 eV (HeNe) excitation source. Similar to the previously reported data observed with the 2.54 eV (Ar ion) excitation energy, these data show an increase in the D-band peak and a decrease in the G'-band peak with decreasing amounts of MWNTs in a sample.[9] This is consistent with the assertion that the D-band results from sp^3 carbon, influenced by the amount of carbon impurities, and the G'-band results from long range order allowing a 2 phonon process to occur.[11] Also observed for the 1.96 eV data, in comparison to the 2.54 eV data, was a down shift in wavenumber for the D-band peak and the G'-band peak to lower wavenumbers (D-band shift from 1352 cm^{-1} to 1325 cm^{-1} and G'-band shift from 2700 cm^{-1} to 2645 cm^{-1}) as seen in Figure 2. The slopes of these changes (47 cm^{-1}/eV and 96 cm^{-1}/eV for the D and G' band respectively) are consistent with the results from work conducted on double resonance theory which predicts a laser-dependent shift in Raman peaks.[11] In comparison the G band shifts little as a function of excitation energy. Fundamentally, the D and G' bands are different from the G band, accounting for the excitation energy dependent results. The D and G' bands are both double resonance processes which have predicted shifts in wavenumber according to the excitation energy, whereas the G band is a single resonance process.[12] These data suggest that the D and G' band intensity ratios stay consistent across excitation energies while the G band intensity is more sensitive across different excitation energies.

APPENDIX B : *Application of the G'/D Raman Ratio for Purity Assessment of Multi-walled Carbon Nanotubes* (MRS Proceedings, San Francisco, California **2007**) Reprint permission from MRS E-Proceedings

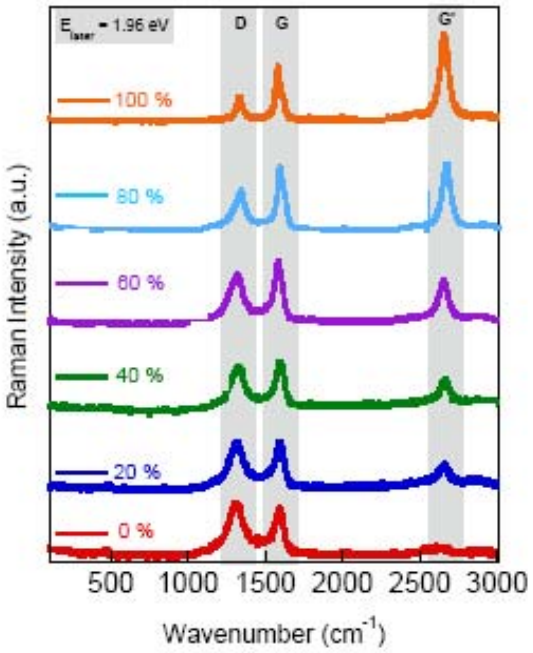

Figure 1. Raman spectra for constructed sample set with an incident laser energy of 1.96 eV. The trends of the D, G, and G' bands are seen in the highlighted regions, and the data are offset for clarity.

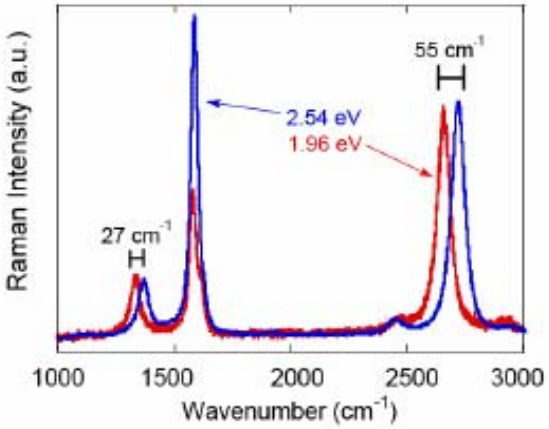

Figure 2. Raman spectra of bulk MWNT powder with 2.54 eV and 1.96 eV excitation energies. Shifts in the D band peak (~ 27 cm^{-1}) and the G'-band (~ 55 cm^{-1}) are shown and the similar ratio trend of the I_G/I_D is seen for both laser energies.

APPENDIX B : *Application of the G'/D Raman Ratio for Purity Assessment of Multi-walled Carbon Nanotubes* (MRS Proceedings, San Francisco, California **2007**) Reprint permission from MRS E-Proceedings

Based upon the spectra in Figure 1, calibration curves were developed from the trends of the ratios of the I_D/I_G, $I_{G'}/I_G$, and $I_{G'}/I_D$. It was observed from the developed calculations of both laser energies that the calibration curves from the $I_{G'}/I_D$ trends were most sensitive across both laser energies due to the largest relative change in the slopes. The data used to calculate the ratios were corrected using a linear baseline subtraction to account for detector background counts and variable sample preparation. In addition, based on the results in Figure 2, the variation in the G band intensity is less attractive for a universal purity assessment technique. Figure 3 shows the data and curve fit (including general equation) corresponding to the $I_{G'}/I_D$ ratio values. Each of the laser excitation data sets were fit independently resulting in a calculated R value greater than 0.99. This goodness-of-fit supports the notion of using a laser excitation energy-independent equation.

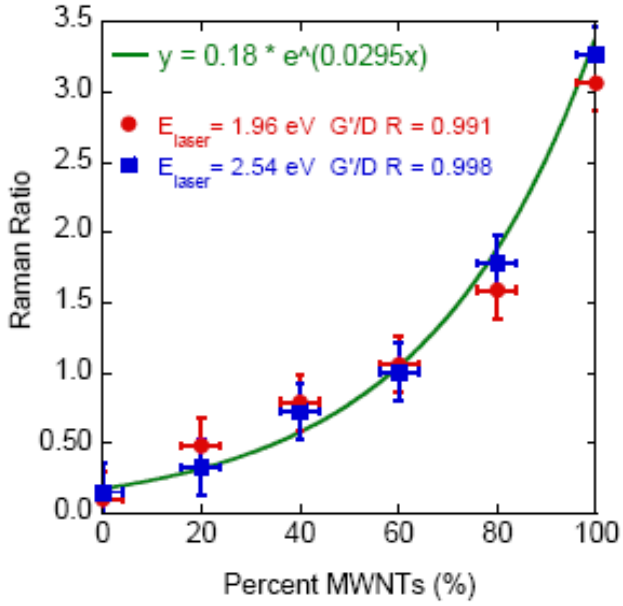

Figure 3. Data points represent the calculated $I_{G'}/I_D$ ratios from the spectra in Figure 1. Data was fitted with exponential curves and calibration equations established from these fits are for calculating purity values.

Previously, we have applied the purity assessment method to bulk MWNTs produced from a design of experiment (DOE) study.[9] Presently, we investigate the use of the relative Raman ratios for directly grown aligned arrays. MWNT aligned arrays were grown on silicon wafers with a native oxide using conditions similar to the 100 % sample in the constructed sample set. The SEM images in Figure 4 depict a representative sample of aligned MWNTs, including the measured height of ~ 300 μm after a 1.5 hour synthesis. The corresponding Raman spectra for this sample are shown in Figure 5 using both excitation lasers. (As noted in Figure 2, the downshift in wavenumber is also observed for the aligned MWNT array sample.) Using the $I_{G'}/I_D$ ratios from each data set, the value of purity was determined to be 75 % for this sample

APPENDIX B : *Application of the G'/D Raman Ratio for Purity Assessment of Multi-walled Carbon Nanotubes* (MRS Proceedings, San Francisco, California **2007**) Reprint permission from MRS E-Proceedings

using the equation in Figure 3. This purity value is consistent across both laser energies. It has been noted that polarization effects can occur when using optical electrical spectroscopy for nanotube characterization; these effects do not greatly affect this present work, but they do hold interesting results for future investigation. The extended purity assessment method is able to effectively quantify the purity of the MWNT aligned arrays.

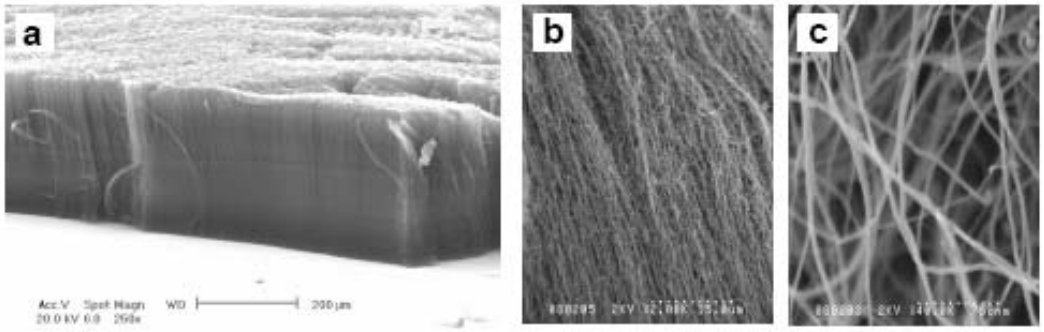

Figure 4. SEM images of MWNT aligned array at magnification (a) 250x (b) 2000x (c) 40000x.

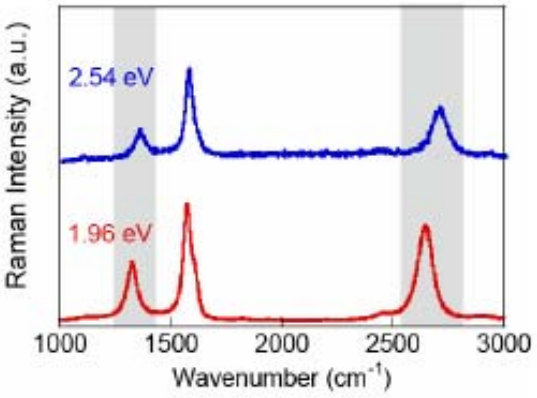

Laser Energy	Raman Ratio ($I_{G'}/I_D$)	Purity (%)
2.54 eV	1.71	76
2.54 eV	1.63	75
1.96 eV	1.63	75
1.96 eV	1.66	75

Figure 5. Raman spectra of MWNT aligned arrays at 2.54 eV and 1.96 eV. The D and G' band are highlighted and the data is offset for clarity. Excitation energies, $I_{G'}/I_D$ Raman peak ratios, and their corresponding purity are to the right.

CONCLUSIONS

Purity assessment of MWNTs using Raman spectroscopy on a constructed sample set has been investigated with a second laser excitation of 1.96 eV. The data show equivalent trends to the 2.54 eV data set in terms of the relative ratios of the D, G, and G'-peaks being correlated to MWNT content. However, the D and G' bands exhibit an excitation energy-dependent Raman shift (27 cm^{-1} and 55 cm^{-1}, respectively), while the G band does not. Given this unique double resonance effect, it was shown that the $I_{G'}/I_D$ ratio is the most sensitive to MWNT purity and results in an excitation-independent equation for purity assessment. This equation has been

APPENDIX B : *Application of the G'/D Raman Ratio for Purity Assessment of Multi-walled Carbon Nanotubes* (MRS Proceedings, San Francisco, California **2007**) Reprint permission from MRS E-Proceedings

applied to calculating the carbonaceous purity of CVD synthesized MWNT aligned arrays grown on SiO_2. A purity value of 75 % was determined for an as-produced aligned array from the Raman spectra, where the energy dependent shifts of the D and G' were also observed. Thus, we have established an equation for purity assessment of MWNTs using the I_G/I_D ratio, which is applicable to bulk powders or aligned arrays and independent of laser excitation (1.96 eV and 2.54 eV).

ACKNOWLEDGMENTS

The authors wish to thank Cory Cress and William Van Derveer for their input during this work. Financial support for this project was made by BP Solar, NASA (SUNY Albany, PI Pradeep Haldar (1046196-2-35652), AFOSR (SUNY Buffalo, PI Paras Prasad) (FA9550-06-0398), NASA (NNC056A60G), and the NRO (RTVGC-05-222). R.A.D. also acknowledges financial support from the Barry M. Goldwater Scholarship.

REFERENCES

1. S. Iijima, *Nature (London)* **354**, 56, (1991).
2. R. P. Raffaelle, B. J. Landi, J. D. Harris, S. G. Bailey, and A. F. Hepp, *Mater. Sci. Eng. B*, **116**, 233, (2005).
3. M. S. Marcus, J. M. Simmons, O. M. Castellini, R. J. Hamers, and M. A. Eriksson, *J. Appl. Phys.* **100**, 084036.1, (2006).
4. Y. Xu, Y. Zhang, E. Suhir, and X. Wang, *J. Appl. Phys.* **100**, 074302.1, (2006).
5. G. L. Zhao, D. Bagayoko, and L. Yang, *J. Appl. Phys.* **99**, 114311.1 (2005).
6. A. Modi, N. Koratkar, E. Lass, B. Q. Wei, and P. M. Ajayan, *Nature (London)* **424**, 171, (2003).
7. J. Li, Q. Ye, A. Cassell, H. T. Nq, R. Stevens, J. Hans, and M. Meyyappan, *Appl. Phys. Lett.* **82**, 2492, (2003).
8. K. L. Jiang, Q. Q. Li, and S. S. Fan, *Nature (London)* **419**, 801 (2002).
9. R. A. DiLeo, B. J. Landi, and R. P. Raffaelle, *J. Appl. Phys.* **101**, 064307, (2007).
10. J. D. Harris, R. P. Raffaelle, T. Gennett, B. J. Landi, and A. F. Hepp, *Mater. Sci. Eng. B*, **116**, 369 (2005).
11. R. Saito *et al., New J. Phys.* **5**, 157.1, (2003).
12. M. Souza *et al., Phys. Rev. B* **69**, 241403, (2004).

APPENDIX C: *Determination of Nanomaterial Energy Levels for Organic Photovoltaics by Cyclic Voltammetry* (Submitted to MRS Proceedings, Boston, Massachusetts **2007**) Reprint permission from MRS E-Proceedings

Mater. Res. Soc. Symp. Proc. Vol. 1031 © 2008 Materials Research Society 1031-H09-54

Determination of Nanomaterial Energy Levels for Organic Photovoltaics by Cyclic Voltammetry

Roberta Ann DiLeo[1], Annick Anctil[2], Brian Landi[1], Cory Cress[2], and Ryne P Raffaelle[1]
[1]Rochester Institute of Technology, Rochester, NY, 14623
[2]Microsystems Engineering, Rochester Institute of Technology, Rochester, NY, 14623

ABSTRACT

A wide variety of nanomaterials and associated nanomaterial/polymer composites are being developed in an effort to produce higher efficiency organic solar cells. This development requires a fundamental understanding of the energy levels for the individual materials, and their composites, to enable device designs which posess appropriate energy level matching. Cyclic voltammetry (CV) allows for the determination of the band gaps (E_g) and energy levels of these various nanomaterials and composites by measuring their oxidation and reduction potentials. These potentials correspond to a given material's ionization potential (IP) and electron affinity (EA), respectively. The results for the EA, IP, and E_g have been determined by CV for derivatized fullerenes and CdSe quantum dots (QD), measured in isolation, and in conjugated polymer composites with MEH-PPV. In addition, CV measurements conducted under dark and illuminated conditions were used to investigate the relationship between energy levels within the composites.

INTRODUCTION

The rapidly growing field of organic photovoltaics (PV) is pushing the limits of achievable efficiencies with conventional materials [1, 2]. The development of high efficiency devices requires an assembly of compatible materials which support photon absorption, exciton diffusion, exciton dissociation, and carrier transport [3]. Choice of suitable materials and their energy level alignments are critical to the development of efficient devices. The enhancement of photon absorption in a device can be accomplished by selecting materials with appropriate band gaps to absorb the solar spectrum. It is also important to minimize recombination sites within the bulk junction; this can be done by avoiding materials which will cause traps due to their unsuitable energy level alignment. Cyclic voltammetry (CV) is a characterization technique that offers the capabilities of probing these important material properties. It is possible to calculate a material's ionization potential (IP) and electron affinity (EA), which correspond to valence states and conduction states, respectively, using CV.

Electrochemical CV measurements can be used to determine these potentials by measuring the voltages at which the material undergoes reduction or oxidation with respect to a reference electrode. These values can be used to calculate the EA and IP of a material as explained by Kucur et al. [4]:

$$EA = -(E_{red} + \Delta E_{vacuum,electrode}) \quad (1)$$

$$IP = -(E_{ox} + \Delta E_{vacuum,electrode}) \quad (2)$$

The band gap (E_g) can be obtained by taking the energy difference of the EA and IP.

APPENDIX C: *Determination of Nanomaterial Energy Levels for Organic Photovoltaics by Cyclic Voltammetry* (Submitted to MRS Proceedings, Boston, Massachusetts **2007**) Reprint permission from MRS E-Proceedings

There have been several reports on the cyclic voltammetry of nanomaterials and polymers commonly used in organic photovoltaics [5-8]. In addition, some research groups have used CV to examine the interaction of CdSe QDs and nanomaterials with polymers in a composite [9-11]. A next step in understanding solar cells is the examination of the pure materials and respective composites under illumination, which yields a representative environment for working devices.

This work has focused on determining the energy levels for a series of CdSe quantum dots, various fullerene derivatives, and the conjugated polymer MEH-PPV (Poly[2-methoxy-5-(2-ethylhexyloxy)-1,4-phenylenevinylene]). CV was used to measure composites of these materials under both dark and illuminated conditions.

EXPERIMENT

CdSe QDs were synthesized using a CdO precursor and were extracted with a mixture of methanol and hexanes as previously reported [12]. A series of four QD sizes were synthesized by varying synthesis time. A ligand exchange of the triocytlphosphine (TOPO) capped QDs was achieved with pyridine, using centrifugation at 6000 rpm for 10 minutes, followed by sonication.

Electrochemical measurements were performed in a three neck cell, under argon, with an electrochemical analyzer from CH Instruments. A rotating platinum disk electrode (Pine Instruments) served as the working electrode, a platinum wire as the counter electrode, and a KCl saturated standard calomel electrode (SCE) as the reference electrode. A 0.1 M solution of acetonitrile and tetrabutylammonium hexafluorophosphate (Aldrich) was used as the electrolyte . Voltammograms were obtained at a scan rate of 20 mV/s and rotation speeds between 50-100 rpm. Illumination studies were performed under dark conditions and under illumination, using halogen lamps (peak λ = 630 nm) and a 350 nm UV lamp. Optical absorption measurements were taken with a Perkin Elmer Lambda 900 (300 to 1600 nm). Fluorescence measurements were taken with a JY-Horiba Fluorolog-3 spectrofluorometer (400 to 800 nm). The reduction and oxidation potentials were used to calculate EA and IP values, respectively.

DISCUSSION

Fig. 1 shows a voltammogram for PCBM C_{60} and the conversion of the two potentials to the respective energy level using a SCE ($\Delta E_{vacuum\ level}$ = 4.158 eV). Fig. 2a shows the optical and fluorescence data for the series of CdSe QDs. The four synthesized dot sizes follow the increasing band gap trend as expected; with smaller dots having a larger band gap. A range of 2.30 to 3.31 nm diameter QDs was calculated based upon Peng's work [13]. Fig. 2b shows the changes in band gap versus QD diameter for optical absorption onsets and peaks, photoluminescence peaks, and electrochemical onsets and peaks. The electrochemical peak values correspond closely with the optical measurements; using the EA and IP peaks rather than the onsets yielded more accurate calculation of band gaps (Fig. 2b). The EA onsets do not change significantly with respect to dot diameter in the electrochemical measurements; whereas the IP onsets change with respect to the band gap (Fig. 2c). In contrast, the EA and IP peak values shift symmetrically with increasing band gap.

APPENDIX C: *Determination of Nanomaterial Energy Levels for Organic Photovoltaics by Cyclic Voltammetry* (Submitted to MRS Proceedings, Boston, Massachusetts **2007**) Reprint permission from MRS E-Proceedings

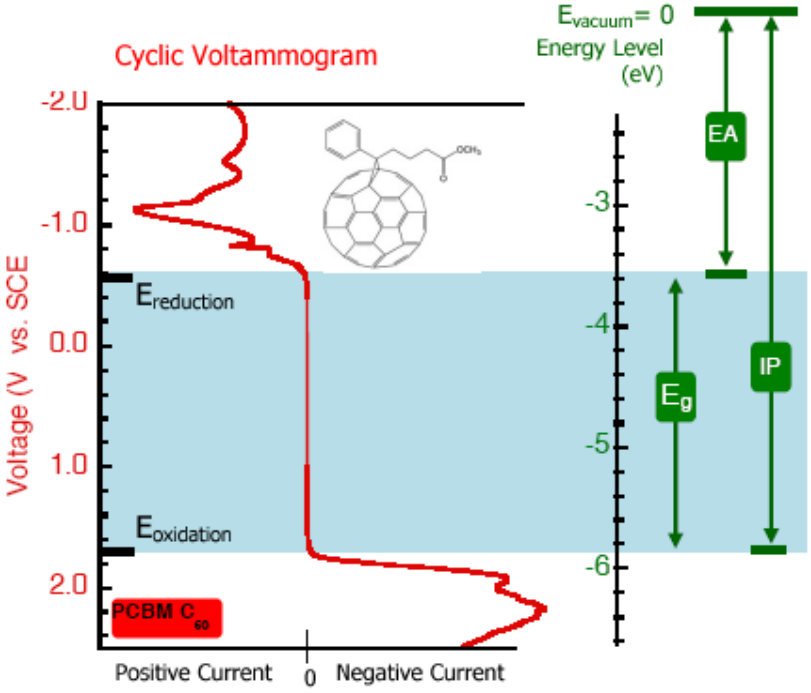

Fig. 1 Representation of a voltammogram of a sample (PCBM C_{60}) and the transition into energy states and band gaps versus vacuum level. (0 V vs. SCE correlates to 4.158 eV with respect to vacuum.)

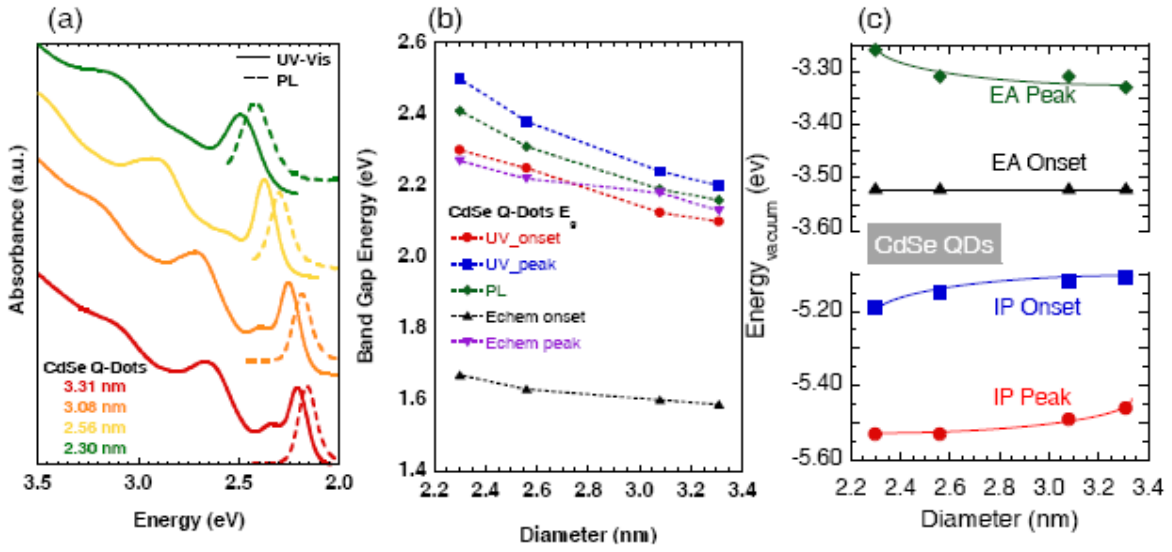

Fig. 2 (a) Optical absorption (solid line) and photoluminescence (dashed line); the QD sizes shown were calculated based upon [13] (b) UV-Vis,, photoluminescence, and electrochemical band gap measurements (c) EA and IP peak and onset values of the QD series. The trend lines in (b) and (c) are guides to the eye.

APPENDIX C: *Determination of Nanomaterial Energy Levels for Organic Photovoltaics by Cyclic Voltammetry* (Submitted to MRS Proceedings, Boston, Massachusetts **2007**) Reprint permission from MRS E-Proceedings

Fullerenes and their derivatives are commonly used in organic PV devices as electron acceptors. These materials have been successfully employed in a variety of organic PV devices [14-17]. The baseline material of PCBM C_{60} ([6,6]-Phenyl C_{61} butyric acid methyl ester) was characterized along with three derivatives (Fig. 3a-d). PCBM C_{70} ([6,6]-Phenyl C71 butyric acid methyl ester), (Fig. 3b) shows different values for energy states as compared to PCBM C_{60} (Fig. 3a), despite the identical derivatized chains on these two materials. This suggests that fullerenes exhibit different electronic energy states, and in the case of these two derivatives the PCBM C_{70} has a shift in the reduction peak as compared to the PCBM C_{60}.

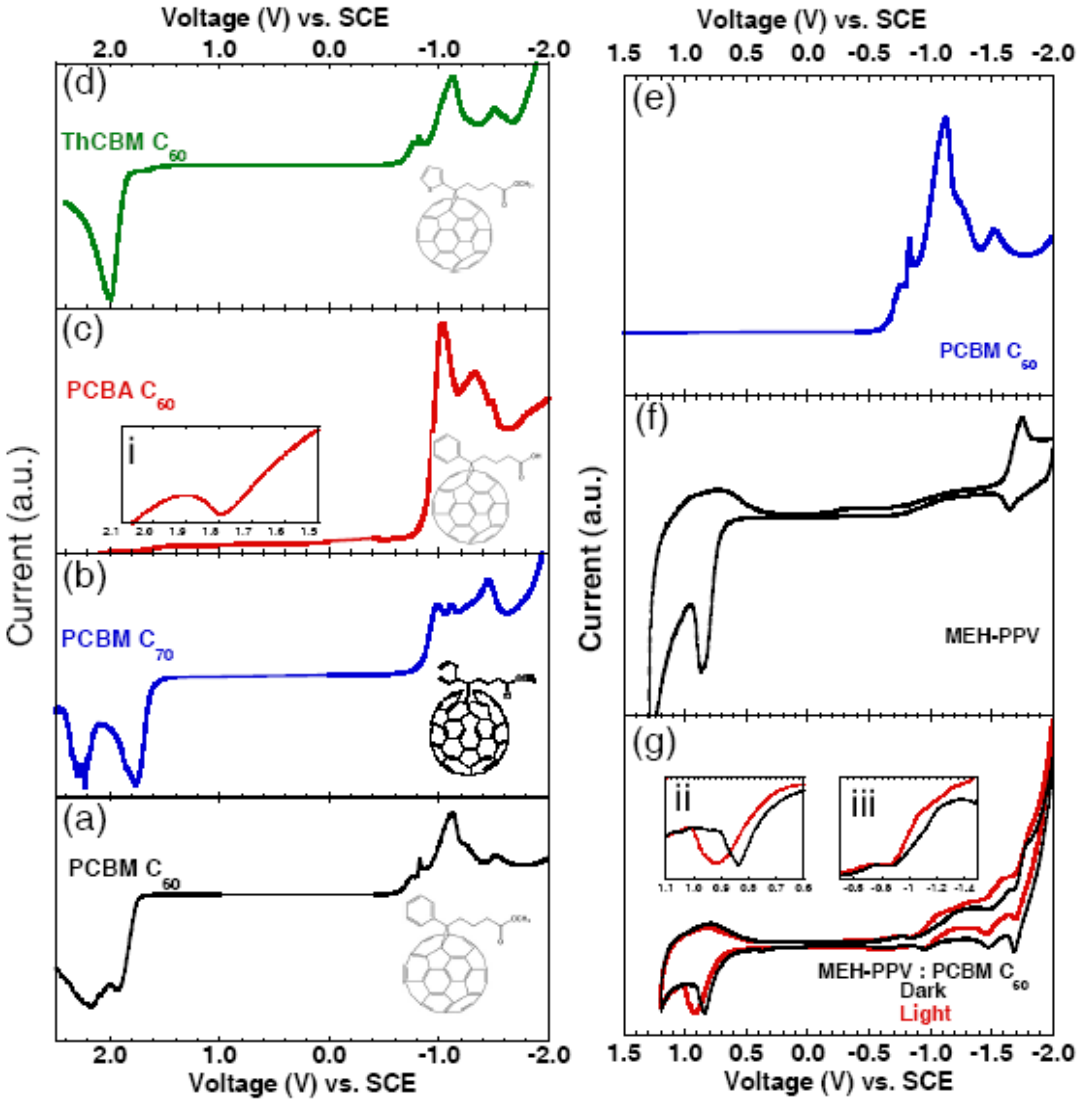

Fig. 3 Voltammagrams of 4 derivatized fullerenes (a) ThCBM C_{60} (i) expanded region of IP (b) PCBA C_{60}, (c) PCBM C_{70}, (d) and PCBM C_{60} (e) PCBM C_{60}, (f) MEH-PPV, (g) MEH-PPV: PCBM C_{60} composite (ii) expanded region of IP (iii) expanded region of of EA

APPENDIX C: *Determination of Nanomaterial Energy Levels for Organic Photovoltaics by Cyclic Voltammetry* (Submitted to MRS Proceedings, Boston, Massachusetts **2007**) Reprint permission from MRS E-Proceedings

The acid derivative PCBA C_{60} ([6,6]-Phenyl C_{61} butyric acid) (Fig. 3c) also shows a shift in the EA and IP values. This shift in energy levels, compared to PCBM C_{60}, for the acid derivative suggests the chain properties play a significant role in the behavior of the molecule. As a fourth derivative, ThCBM C_{60} (1-(3-methoxycarbonyl) propyl-1-thienyl-[6,6]-methanofullerene) (Fig. 3d) gives rise to behavior similar to PCBM C_{60}, with an EA of -3.50 eV versus the vacuum level, suggesting the substituted ring structure (i.e. phenyl vs. thiophene) has little bearing on EA value for this structure. However, there is an observable change in the IP values upon the thiophene substitution. Fig. 3e and 3f shows the voltammograms of the pure PCBM C_{60} and pure polymer, respectively. The voltammogram of the composite is given in Fig. 3g. The observed energy states in this material are a result of assimilation and shifting of the pure materials' energy states.

Fig. 3g also shows the effects on the MEH-PPV : PCBM C_{60} Composites when the CV is performed under illumination. There is a clear shift to more positive voltage in the IP when the composite is illuminated (Fig. 3gii). A smaller shift in the EA is also observed as shown in Fig. 3giii. This series of CV measurements is summarized in Fig. 4. Although it would not be expected, it is clear from this data that the states observed in the composite are not merely a superposition of the pure materials. The effects on energy levels due to illumination of the composite are also shown red.

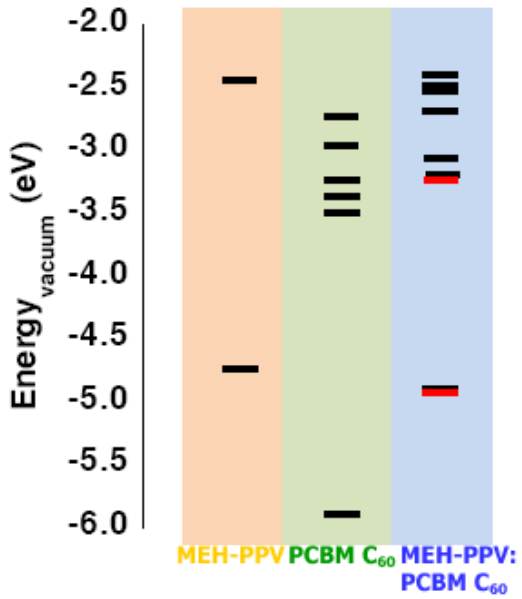

Fig. 4 Energy level cascade of pure PCBM C_{60}, MEH-PPV, and the composite material versus vacuum level. Red bands correspond to shifts due to illumination

CONCLUSIONS

CV was performed on some nanomaterials, polymers and their composites that are commonly used in the fabrication of organic photovoltaics. A series of CdSe QDs with differing diameters was studied. It was shown that for increasing band gap (decreasing dot size) the EA onset remains relatively constant while the IP onset shifts according to band gap. Conversely,

the EA and IP peak values shift symmetrically with band gap. The results from the series of fullerene derivatives suggest that both fullerene size and chain composition influence the behavior of energy states. Materials in their pure states were investigated and compared to resulting composites in MEH-PPV. The measurements made on these composites are indicative of energy state behaviors in a device structure. Composite materials were also investigated using controlled illumination environments and shown to exhibit different behaviors under illumination. It was shown for the MEH-PPV: PCBM C_{60} blend that shifts occur in both the EA and IP values, under illumination.

ACKNOWLEDGMENTS

Financial support for this project was made by BP Solar, AFOSR (SUNY Buffalo, PI Paras Prasad) (FA9550-06-0398).

REFERENCES

1. Forrest, S.R., MRS Bulletin, 2005. **30**: p. 28-32.
2. Koster, L.J.A., et al., Physical Review B, 2005. **72**: p. 085205-1-9.
3. Lemaur, V., et al., Journal of American Chemical Society, 2005. **127**: p. 6077-86.
4. Kucur, E., et al., Journal of Chemical Physics, 2003. **119**(4): p. 2333-2337.
5. Zhang, H., et al., Journal of Applied Polymer Science, 2005. **100**: p. 3634-3640.
6. Holt, A.L., J.M. Leger, and S.A. Carter, Journal of Chemical Physics, 2005. **123**: p. 044704-1-7.
7. Kim, J.H. and H. Lee, Chemical Materials, 2002. **14**: p. 2270-2275.
8. Richter, M.M., et al., Chemical Physics Letters, 1994. **226**: p. 115-120.
9. Ding, H., et al., Electrochemistry Communications, 2002. **4**: p. 503-505.
10. Kucur, E., et al., Journal of Chemical Physics, 2004. **120**: p. 1500-1505.
11. Sonar, P., et al., Materials Research Bulletin, 2006. **41**: p. 198-208.
12. Landi, B.J., et al., Materials Letters, 2006. **60**: p. 3502-3506.
13. Yu, W.W., et al., Chemistry of Materials, 2003. **15**: p. 2854-2860.
14. Backer, S.A., et al., Chemical Materials, 2007. **19**: p. 2927-2929.
15. Benson-Smith, J.J., et al., Advanced Functional Materials, 2007. **17**: p. 451-457.
16. Kooistra, F.B., et al., Organic Letters, 2006. **9**: p. 551-554.
17. Zheng, L., et al., Journal of Physical Chemistry B, 2004. **108**: p. 11921-11926.

REFERENCES

1. Raffaelle, R.P., B.J. Landi, J.D. Harris, S.G. Bailey, and A.F. Hepp, Material Science & Engineering B, 2005. **116**: p. 233-243.
2. Landi, B.J., R.A. DiLeo, C.M. Schauerman, C.D. Cress, M.J. Ganter, and R.P. Raffaelle, Journal of Nanoscience and Nanotechnology.
3. Forrest, S.R., MRS Bulletin, 2005. **30**: p. 28-32.
4. Li, J. and L.-W. Wang, Chemical Materials, 2004(16): p. 4012-4015.
5. Lemaur, V., M. Steel, D. Beljonne, J.-L. Bredas, and J. Cornil, Journal of American Chemical Society, 2005. **127**: p. 6077-86.
6. Iijima, S., Nature, 1991. **354**: p. 56-58.
7. Marcus, M.S., Simmons, J.M., Castellini, O.M., Hamers, R.J., Eriksson, M.A., Journal of Applied Physics, 2006. **100**: p. 084306-1 - 084306-6.
8. Xu, Y., Zhang, Y., Suhir, E., Wang, X., Journal of Applied Physics, 2006. **100**: p. 074302-1-074302-5.
9. Zhao, G.L., Bagayoko, D., Yang, L., Journal of Applied Physics, 2006. **99**: p. 114311-1 -114311-5.
10. Landi, B.J., Ruf, H.J., Evans, C.M., Cress, C.D., Raffaelle, R.P., Journal of Physical Chemistry B, 2005. **109**: p. 9952-9965.
11. Benoit, J.M., J.P. Buisson, O. Chauvet, C. Gordon, and S. Lefant, Physical Review B, 2002. **66**: p. 073417-1-073417-4.
12. Huang, W., Y. Wang, G. Luo, and F. Wei, Carbon, 2003. **41**: p. 2585-2590.
13. Keszler, A.M., L. Nemes, S.R. Ahmad, and X. Fang, Journal of Optoelectronics and Advanced Materials, 2004. **6**: p. 1269-1274.
14. McKee, G.S.B. and K.S. Vecchio, Journal of Physical Chemistry B, 2005. **110**: p. 1179-1186.
15. Murphy, R., J.N. Coleman, M. Cadek, B. McCarthy, M. Bent, A. Drury, R.C. Barklie, and W.J. Blau, Journal of Physical Chemistry B, 2001. **106**: p. 3087-3091.
16. Zhao, X., Y. Ando, L.C. Qin, H. Kataura, Y. Maniwa, and R. Saito, Physica B, 2002. **323**: p. 265-266.
17. Saito, R., A. Gruneis, G.G. Samsonidze, V.W. Brar, G. Dresselhaus, M.S. Dresselhaus, A. Jorio, L.G. Cancado, C. Fantini, M.A. Pimenta, and A.G. Souza-Filho, New Journal of Physics, 2003. **5**: p. 157.1-157.15.
18. Zhang, H., X. Huang, L.Z. Fan, B. Nin, Y.Q. Wu, L.P. Zheng, and Y. Cao, Journal of Applied Polymer Science, 2005. **100**: p. 3634-3640.
19. Holt, A.L., J.M. Leger, and S.A. Carter, Journal of Chemical Physics, 2005. **123**: p. 044704-1-7.
20. Kim, J.H. and H. Lee, Chemical Materials, 2002. **14**: p. 2270-2275.
21. Richter, M.M., F.-R.F. Fan, F. Klavetter, A.J. Heeger, and A.J. Bard, Chemical Physics Letters, 1994. **226**: p. 115-120.
22. Ding, H., P. Bertoncello, M.K. Ram, and C. Nicolini, Electrochemistry Communications, 2002. **4**: p. 503-505.

23. Kucur, E., J. Riegler, G.A. Urban, and T. Nann, Journal of Chemical Physics, 2004. **120**: p. 1500-1505.
24. Sonar, P., K.P. Sreenivasan, T. Madddanimath, and K. Vijayamohanan, Materials Research Bulletin, 2006. **41**: p. 198-208.
25. Harris, J.D., Raffaelle,R.P., Gennett, T., Landi, B.J., Hepp, A.F., Material Science & Engineering B, 2005. **116**: p. 369-374.
26. Kucur, E., J. Riegler, G.A. Urban, and T. Nann, Journal of Chemical Physics, 2003. **119**(4): p. 2333-2337.
27. Landi, B.J., C.M. Evans, J.J. Worman, S.L. Castro, S.G. Bailey, and R.P. Raffaelle, Materials Letters, 2006. **60**: p. 3502-3506.